

3<sup>rd</sup> International Accelerator School for Linear Collider

Illinois, USA

**LINAC-I**

Lecture Notes

Oct. 21, 2008

Toshiyasu Higo

KEK

# Contents of LINAC-I

1. Acceleration to higher energy
  - 1.1 Linac requirements for linear collider
  - 1.2 Development of linear accelerators and extension to linear collider
  - 1.3 RF acceleration
  - 1.4 Scope of this lecture
  - 1.5 Typical parameters of the present two designs
  
2. Maxwell's equation and microwave transmission
  - 2.1 Maxwell's equation to wave equation
  - 2.2 Wave propagation in a uniform waveguide
  - 2.3 Wave propagation in a periodically loaded waveguide
  
3. Cavity as a unit of acceleration
  - 3.1 Inside a cavity
  - 3.2 Frequency
  - 3.3 Acceleration related parameters
  - 3.4 R/Q
  - 3.5 Surface loss and Q value
  - 3.6 Cares on local field
  
4. Coupled cavity system in a SW regime
  - 4.1 Coupled resonator model
  - 4.2 Perturbation analysis
  - 4.3 Choice of acceleration mode
  - 4.4 Some analysis of nine cell SCC cavity
  
5. Pillbox as a simple base to represent practical cavities
  - 5.1 Pillbox cavity expression
  - 5.2 Q of a pillbox cavity
  - 5.3 R/Q of a pillbox cavity
  
6. Circuit modeling of a cavity
  - 6.1 Cavity field to equivalent circuit

6.2 Cavity response expression in the phasor diagram

6.3 Transient response

7. Travelling wave linac

7.1 SW and TW

7.2 Acceleration in TW and related parameters

7.3 Modes in DLS, disk-loaded structure

7.4 DLS basic design variables

7.5 Energy gain expression, especially CG case

7.6 Beam loading

7.7 Transient properties of microwave propagation

7.8 Reflection from cell perturbation and tuning

8. Summary of LINAC-I

## Chapter 1 Acceleration to higher energy

### 1.1 Linac requirements for linear collider

The collision energy in linear collider, LC, is simply described as

$$e E_c = e E_a L_{linac} = \frac{P_{linac} \eta_{RF \rightarrow Beam}}{N N_b F_{rep}} ,$$

where  $N$  is the number of particles per bunch,  $N_b$  number of bunches in a train,  $F_{rep}$  the repetition rate of the linac and  $P_{linac}$  the RF power of whole linac. In a given linac length, the acceleration gradient  $E_a$  should be large enough to reach the required collision energy. This is the theme of almost all of the linear accelerators. From field and power relation, the required power is proportional to square of acceleration gradient,  $E_a$ . Therefore, it is required to have a huge power as the field goes to higher and higher and eventually there appears a limit from this. In addition, it is required to make the power transfer efficiency from wall plug to RF power and also RF power into beam power high enough to suppress the total linac power consumption within a practical limit. In the lecture LINAC-I, we review how the microwave power transfers into beam effectively. The power generation scheme is not described in this lecture.

On the other hand, the luminosity  $L$  is another key parameter to make the collision experiment realistic. The luminosity is described as

$$\frac{L}{P_{linac}} = \frac{L_0 N_b F_{rep}}{e E_c N N_b F_{rep} / \eta_{RF \rightarrow Beam}} = \frac{1}{e E_c} \frac{L_0}{N} \eta_{RF \rightarrow Beam} ,$$

where  $L_0$  is the luminosity for each bunch crossing. The high  $L_0$  is crucial and here the beam size at the collision point plays an essential role. In the lecture LINAC-II, we describe how to preserve the low emittance beam through the linac.

### 1.2 Development of linear accelerators and extension to linear collider

The linear accelerator (linac) to date is the history of the tool to reach the energy as high as possible. About thirty years after the electron was identified in a cathode ray tube in 1896, the RF linear acceleration schemes were proposed and tested in around 1930. For the acceleration of slow particles with its velocity much less than light velocity,  $0.005c \sim 0.1c$ , such early linear accelerators are based on the electrodes and drift tube, such as those by Wideröe or that by Sloan and Laurence. The acceleration is controlled with electrically phased forced excitation of the electrodes. For higher velocity particles, the Alvarez cavity is used where the whole cavity (tank) is resonant in a certain mode of the tank and the decelerating field is shielded from the beam by drift tubes. Then after, the

coupled resonator type linear accelerators have been developed for even higher energy particles, such as 1GeV protons, with improving the shunt impedance, a measure of beam acceleration w.r.t. the drive power. To reach much higher energy in electrons, the travelling wave accelerators based on disk-loaded structures were constructed. The electron energy reached 1GeV level in 1955.

The acceleration in the linear accelerator is only once while passing through the linac. In order to increase the particle energy with limited number of acceleration cavities, the ring accelerator was developed. The synchrotron accelerated electron and positrons up to as high as 100GeV at LEP. In the LEP RF acceleration to keep as much as high energy as possible, the large RF acceleration voltage per turn is crucial even though it is ring machine. It is because the synchrotron light emission,  $SR$ , increases severely as energy  $E$  but moderately as the ring radius  $\rho$  increases<sup>1</sup>.

$$SR \propto \frac{E^4}{\rho}$$

To realize high acceleration voltage in LEP, the accelerating cavity is equipped with an energy storage cavity where the microwave energy is stored during the beam is outside cavity, while the energy flows into accelerating cavity when the beam comes back to the cavity. This is one of the ways to save power to reach higher energy. For further increase stored beam energy, the LEP replaced the normal conducting cavities by superconducting cavities to more effectively transfer microwave power into beam. With this change, the LEP reached 100GeV beam in a 27km ring.

Since the LEP size is the practical limit, the higher energy machine than LEP with such light particles as electrons should be realized only by the linear accelerator, where there is no energy loss due to the synchrotron light emission and all the energy acquired to beam can be added linearly. Therefore, in order to aim at such collision energy as 200GeV or more, the linear accelerator plays an essential role again for the electron colliding machine.

The cavities for high current machine need other case on beam stability. An example is shown in the ARES cavity<sup>2</sup> for KEKB. In this cavity system, each accelerating cell is equipped with a storage cavity, such as the case of LEP<sup>3</sup>. However, this storage cavity stores large energy to make the microwave performance of the cavity/beam system stable by making the amount of energy exchange with beam is much less than the stored energy by the system. Various ways to suppress such beam cavity interactions causing beam instability in the ring is one of the key demands for the high current ring machine, while the suppression of the beam cavity interaction, such as those due to the higher modes in the cavities, plays an essential role also in the linear accelerators. This is because even a small perturbation can be grown resonantly in a very long linac. The beam blowup phenomena, BBU, observed in early SLAC two mile accelerator is one of the typical examples.

As the LC requires high energy, the acceleration gradient is one of the most relevant parameters for the linac design. Even assuming that the enough power is available to sustain the high gradient, the acceleration system needs such consideration, much of which we described in the lecture.

Problems relevant to high gradient are such as

- Breakdowns due to high electromagnetic field in the cavity,
- Quenching of superconducting material due to high magnetic field or high heat load,
- Mechanical vibration of cavity due to Maxwell's stress,
- Temperature rise only at the inner surface of the cavity,
- Field emission and dark current to be accelerated by the cavity,
- Multipacting and associated thermal and electrical difficulties,
- etc. etc.

and some of these are briefly reviewed in the lecture.

### ***1.3 RF acceleration***

It is the simplest way to accelerate a charged particle by putting it between two electrodes sustaining a DC electric field. The energy accepted by the particle is the sum of potential difference between the electrodes and the charge of the accelerated particle. However to reach higher energy, it is clear that the acceleration between the finite number of electrode sets is not enough. The more energy is obtained naturally by using an alternating field, RF (radio frequency) in a microwave regime. If we talk about the acceleration of  $\beta=1$  particle in a practical size of say one foot, the half period of the RF should be about the transit time of the particle over the size, 1nsec. This means the frequency of the RF will be of the GHz range.

One of the ways to accelerate the particle continuously along the linac is the surfing mechanism for the particle sitting on the crest of RF field and travelling synchronously in phase with the travelling RF wave (TW). On the other hand, in an alternating field staying at the same position in space, the standing wave (SW), the acceleration occurs when the field is at the right direction and the direction of the field is reversed after the beam arrives at the exit of the acceleration unit, the accelerator cell or acceleration cavity. This is done by the frequency tuning and the cavity positioning. Both SW and TW can be applied for linearly located cavities in linac and for the cavity in the ring.

### ***1.4 Scope of this lecture***

In the present lecture, we take the two types of linear accelerators being developed now for LC in order to describe the basic ideas of linear accelerators. These are the two choices different in various viewpoints such as;

Project; ILC and CLIC

Energy filling mechanism; standing wave (SW) and travelling wave (TW)

Cavity power loss mechanism; superconducting (SC) and normal conducting (NC)

Frequency range; 1.3GHz (L-band) and 11~12GHz (X-band)

Acceleration gradient; 31.5MV/m and 100MV/m  
etc.

The pros and cons for each case should be understood so that the practical accelerator can be designed satisfying the physics demand as much as possible. However, these two types both apply the RF acceleration, the electromagnetic field in a microwave range, which is focused to the beam passage area confined by solid materials. In this sense, the two cases have the same kind of problems arising from the difficulties in the realization of the ideal material property. Once the material behaves well sustaining the high gradient, the size of the linac components can be 10cm to 1cm so that the components of linac are managed to be made from the present-day state of the art of the present-day mechanical engineering. This lecture is designed to present the basic understanding for the linear accelerators by discussing the similarities and differences of the two types.

The acceleration at much higher gradient level, 1~10GV/m, with such an acceleration in plasma wave, has already been proved over a short distance of cm level. However, the author thinks the technology needs to be further developed in many years before applying to the actual LC linac design. In this context, the next LC in ten year time scale should be based on the classical microwave acceleration mechanism, which we cover in this lecture.

### ***1.5 Typical parameters of the present two designs***

The typical linac parameters of the two designs, ILC and CLIC, relevant to the present lecture are listed for 500GeV c.m. energy case in the table of the following page. There are huge differences in acceleration RF related parameters and beam structure between the two cases, while the beam qualities such as emittances of the two cases are close. Following are some of the comparisons;

Acceleration field; comparable,  
Beam emittance; comparable,  
Beam current; ILC  $\ll$  CLIC by 100,  
Pulse length; ILC  $\gg$  CLIC by 10000,  
Number of bunches in a train; ILC  $>$  CLIC by 10,  
Peak power per cavity; ILC  $\ll$  CLIC by 1000,  
Rep. rate; ILC  $<$  CLIC by 10,  
Bunch spacing w.r.t. RF period; ILC  $\gg$  CLIC by 100,  
Number of cells per cavity; comparable;  
RF frequency; ILC  $<$  CLIC by 10,  
Cavity aperture / wavelength; comparable

These parameters are closely related to the design of the linac and are described in the lecture.

Table of relevant parameters of two LC design

| Parameters                           |                       | units         | ILC(RDR)  | CLIC(500) |
|--------------------------------------|-----------------------|---------------|-----------|-----------|
| Injection / final linac energy       | $E_{\text{linac}}$    | GeV           | 25 / 250  | / 250     |
| Acceleration gradient                | $E_a$                 | MV/m          | 31.5      | 80        |
| Beam current                         | $I_b$                 | A             | 0.009     | 2.2       |
| Peak RF power / cavity               | $P_{\text{in}}$       | MW            | 0.294     | 74        |
| Initial / final horizontal emittance | $\epsilon_x$          | $\mu\text{m}$ | 8.4 / 9.4 | 2 / 3     |
| Initial / final vertical emittance   | $\epsilon_y$          | nm            | 24 / 34   | 10 / 40   |
| RF pulse width                       | $T_p$                 | $\mu\text{s}$ | 1565      | 0.242     |
| Repetition rate                      | $F_{\text{rep}}$      | Hz            | 5         | 50        |
| Number of particles in a bunch       | $N$                   | $10^9$        | 20        | 6.8       |
| Number of bunches / train            | $N_b$                 |               | 2625      | 354       |
| Bunch spacing                        | $T_b$                 | ns            | 360       | 0.5       |
| Bunch spacing per RF cycle           | $T_b / T_{\text{RF}}$ |               | 468       | 6         |
| Frequency                            | $F$                   | GHz           | 1.3       | 12        |
| Beam phase w.r.t.RF                  |                       | degree        | 5         | 15        |
| EM mode in cavity                    |                       |               | SW        | TW        |
| Number of cells in a cavity          |                       |               | 9         | 19        |
| Cavity beam aperture                 | $a/\lambda$           |               | 0.152     | 0.145     |
| Bunch length                         | $\sigma_z$            | mm            | 0.3       | 0.044     |



## Chapter 2 Maxwell's equation and microwave transmission

### 2.1 Maxwell's equation to wave equation

Maxwell's equation in a continuum media is the very basic for the design of microwave system for the RF acceleration of linear accelerator. Four equations<sup>4</sup> are as follows;

$$\begin{aligned}
 (1) \quad \nabla \cdot D &= \rho \\
 (2) \quad \nabla \cdot B &= 0 \\
 (3) \quad \nabla \times E &= -\frac{\partial B}{\partial t} \\
 (4) \quad \nabla \times H &= j + \frac{\partial D}{\partial t}
 \end{aligned} \tag{2-1}$$

If all the quantities vary harmonically in time, as almost always the case for the RF acceleration in lineac,

$$E = E_0 e^{j\omega t} \quad \text{and} \quad H = H_0 e^{j\omega t} \tag{2-2}$$

Then Maxwell's equations become

$$\begin{aligned}
 \nabla \times E &= -j\omega\mu H \\
 \nabla \times H &= (\sigma + j\omega\varepsilon) E
 \end{aligned} \tag{2-3}$$

These have a solution of the wave propagating along the z-direction,

$$\begin{aligned}
 E &= E_0 e^{i\omega t - \gamma_0 z} \\
 H &= H_0 e^{i\omega t - \gamma_0 z}
 \end{aligned} \tag{2-4}$$

where

$$\gamma_0 = \alpha_0 + j\beta_0 = \sqrt{-\omega^2 (\varepsilon - j\sigma/\omega)\mu} \tag{2-5}$$

The  $\gamma_0$  is the propagation constant, where  $\alpha_0$  is related to the attenuation along the passage, while  $\beta_0$  the wave number, the phase advance, along the propagation direction.

We define the wave impedance  $Z_0$  to be the ratio of electric field / magnetic field

$$Z_0 = E_x / H_y \tag{2-6}$$

and assume the plane wave propagating in z-direction with  $E_x$  and  $H_y$  component,

$$E = (E_x, 0, 0), \quad H = (0, H_y, 0) \tag{2-7}$$

Then the first of eq. (2-3) becomes

$$\begin{aligned}
 \nabla \times (\vec{k}_x E_x, 0, 0) &= -j\omega\mu (0, \vec{k}_y H_y, 0) \\
 \therefore \frac{\partial}{\partial z} E_x &= -\gamma E_x = -j\omega\mu H_y
 \end{aligned} \tag{2-8}$$

Then finally we get  $Z_0$  as

$$Z_0 = \frac{E_x}{H_y} = \frac{j\omega\mu}{\gamma} = \sqrt{\frac{\mu}{\epsilon - \frac{j\sigma}{\omega}}} \quad (2-9)$$

In an insulated material, including the vacuum,  $\sigma=0$  so that

$$\gamma_0 = j\omega\sqrt{\epsilon\mu} \quad (2-10)$$

and this is the propagation with a velocity

$$v = 1/\sqrt{\epsilon\mu} \quad (2-11)$$

in free space. The wave impedance, defined as the ratio of electric field / magnetic field becomes

$$Z_0 = E_x / H_y = \sqrt{\frac{\mu}{\epsilon}} = 377 \Omega \quad (2-12)$$

Using  $Z_0$  and  $\gamma_0$  in Maxwell's equations (3) and (4) become

$$\begin{aligned} \nabla \times E &= -\gamma_0 (Z_0 H) \\ \nabla \times (Z_0 H) &= \gamma_0 E \end{aligned}$$

From these equations, we obtain the wave equations,

$$\begin{aligned} \Delta E - \gamma_0^2 E &= 0 \\ \Delta H - \gamma_0^2 H &= 0 \end{aligned} \quad (2-13)$$

Here the following vector relation is applied.

$$\nabla \times \nabla \times \vec{A} = \nabla (\nabla \cdot \vec{A}) - \Delta \vec{A} \quad (2-14)$$

On the contrary in a poor conductor, the following condition applies;

$$\sigma / \omega \ll \epsilon \quad (2-15)$$

and the propagation constant becomes

$$\gamma_0 = \frac{1}{2}\sigma\sqrt{\frac{\mu}{\epsilon}} + j\omega\sqrt{\epsilon\mu} \quad (2-16)$$

This is the lossy propagation with the same phase advance as in the non-conducting medium but with the attenuation due to finite conductivity  $\sigma$ . This sometimes appears in a lossy material to absorb microwave in modes outside of the acceleration field.

Finally let us consider the case with a good conductor but not infinitely conductive one.

$$\sigma / \omega \gg \epsilon \quad (2-17)$$

Actually in copper case,  $\sigma(\text{Cu})=5.8 \times 10^7 [1/\Omega/\text{m}]$ , the condition of good conductor is actually satisfied as  $\varepsilon\omega/\sigma=10^{-8} \ll 1$  at 12GHz. This condition appears in many of the acceleration system components. In this case, the propagation constant and the wave impedance become

$$\gamma_m = \sqrt{j\omega\mu\sigma} = (1+j)\sqrt{\frac{\sigma\omega\mu}{2}} \quad (2-18)$$

And from eq. (2-9), the wave impedance in the medium becomes

$$Z_m = \frac{j\omega\mu}{\gamma} = \sqrt{\frac{j\omega\mu}{\sigma}} = (1+j)\sqrt{\frac{\omega\mu}{2\sigma}} \quad (2-19)$$

From  $\gamma_m$ , the attenuation exists, which scales as the square root of conductivity. This means that the propagation to this medium is attenuated faster in higher conductive material. From the wave impedance  $Z_m$  form, the electric field and magnetic field is separated by 45 degrees in phase.

When we consider a plane wave injecting to such medium in z-direction<sup>5</sup> as shown in the Fig. 1, the injected wave propagates in the medium is described as

$$E_x / H_y \equiv Z_m = (1+j)\sqrt{\frac{\omega\mu}{2\sigma}} \quad (2-20)$$

so that the E field in the medium becomes very small as conductivity  $\sigma$  increases. The wave equation in the medium becomes,

$$\Delta E_t - \gamma_0^2 E_t = \left( \frac{\partial^2}{\partial z^2} - j\omega\mu\sigma \right) E_t = 0 \quad (2-20)$$

so that the field is expressed as

$$E_t = E_s e^{-\gamma z} \quad (2-21)$$

where

$$\gamma = (j\omega\mu\sigma)^{1/2} = \frac{1+j}{\delta_s} \quad \text{with} \quad \delta_s = \sqrt{\frac{2}{\sigma\omega\mu}} \quad (2-22)$$

The field is attenuated exponentially with the decay constant of skin depth,  $\delta_s$ . At 12 GHz in copper, it becomes ~0.6 micron. If the surface is deformed or rough in a micron level, we should care about the larger surface area than the case of perfectly flat case. It is to be noted that most of the incident wave is reflected back to vacuum as shown in the figure because the wave impedance of vacuum,  $377\Omega$  is very different from that in this

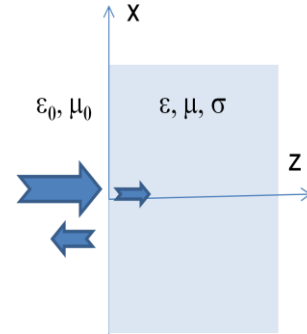


Fig. 1

medium, about 40 mΩ in copper case. Here the reflection coefficient  $\Gamma$  and the associated transmission coefficient are described as

$$\Gamma = \frac{Z_m - Z_0}{Z_m + Z_0} \approx -1, \quad T = 1 + \Gamma = \frac{2Z_m}{Z_m + Z_0} \approx \frac{1}{5000} \ll 1 \quad (2-23)$$

The corresponding magnetic field in the medium is expressed as

$$H_t \equiv \frac{1}{-j\omega\mu} \nabla \times E_t = \frac{\gamma}{j\omega\mu} E_s e^{-\gamma z} \quad (2-24)$$

where the surface field  $E_s$  is related to the incident wave amplitude  $E_0$  as

$$\begin{aligned} E_s &= (1 + \Gamma) E_0 = T E_0 \\ Z_0 H_s &= (1 - \Gamma) Z_0 H_0 = T Z_0 H_0 \end{aligned} \quad (2-25)$$

The  $H_t$  field in the medium behaves as exponential decaying property into the medium the same as the  $E_t$  field. If we integrate the current and name it as the surface current,  $J_s$  [A/m], it becomes, with using eqs. (2-19), (2-23) and (2-25),

$$J_s \equiv \int_0^\infty \sigma E(z) dz = \frac{\sigma E_s}{\gamma} = \frac{2E_0}{Z_m} [A/m] \quad (2-26)$$

and we can express that the magnetic field is terminated by this surface current. From eq. (2-25), surface magnetic field is

$$H_s \approx 2H_0 \quad (2-27)$$

and the value in (2-26) is the same as this surface magnetic field. The loss in such as the actual cavity is expressed as the ohmic loss of this current with the impedance  $R_s$ ,

where

$$R_s = \sqrt{\frac{\omega\mu}{2\sigma}} \quad (2-28)$$

## 2.2 Wave propagation in a uniform waveguide

Let us consider the case of the wave propagation along some guided channel extending toward z-direction. Here we formalize with the form

$$E = E_0 e^{i\omega t - \gamma z} \quad H = H_0 e^{i\omega t - \gamma z} \quad (2-29)$$

so that the wave equation becomes

$$\nabla_t^2 E_0 + (\gamma^2 - \gamma_0^2) E_0 = 0 \quad (2-30)$$

This equation can be solved with a proper cutoff propagation constant,

$$\beta_c^2 = \gamma^2 - \gamma_0^2 \quad (2-31)$$

and especially in non-conducting medium the propagation constant becomes

$$\gamma^2 = \beta_c^2 - \omega^2 \varepsilon \mu \quad (2-32)$$

If  $\omega < \omega_c = \beta_c / \sqrt{\varepsilon \mu}$ , then  $\gamma$  becomes real and it means that the wave cannot propagate along such a transmission line. The  $\omega_c$  is called the cutoff frequency. There are number of modes which satisfy the above Laplace eq. (2-30) and the cutoff frequency and propagation constant depends on the choice of the mode. Lowest propagating mode is called “dominant mode.” The propagation at a frequency higher than the cutoff of the second mode occur with some mixing of the possible transmission modes and we should be careful how to keep the wanted mode.

Let us write the field decomposing it into transverse component and longitudinal one.

$$\begin{aligned} E &= (\vec{k}_t E_t + \vec{k}_z E_z) e^{i\omega t - \gamma z} \\ H &= (\vec{k}_t H_t + \vec{k}_z H_z) e^{i\omega t - \gamma z} \end{aligned} \quad (2-31)$$

For the longitudinal components,

$$\begin{aligned} \nabla^2 E_z + \beta_c^2 E_z &= 0 \\ \nabla^2 H_z + \beta_c^2 H_z &= 0 \end{aligned} \quad (2-32)$$

Once we obtain these longitudinal components, we can derive the transverse components from Maxwell's equation as

$$\begin{aligned} E_t &= \frac{-\gamma}{\beta_c^2} \nabla E_z + \frac{\gamma_0}{\beta_c^2} (k_z \times \nabla Z_0 H_z) \\ Z_0 H_t &= \frac{-\gamma}{\beta_c^2} \nabla Z_0 H_z - \frac{\gamma_0}{\beta_c^2} (k_z \times \nabla E_z) \end{aligned} \quad (2-33)$$

We can choose either  $E_z=0$  or  $H_z=0$  and the former makes TE (transverse electric) mode or H mode and the latter TM (transverse magnetic) mode or E mode. If the waveguide cross-section varies along z-direction, the TE and the TM are not purely exists and the mixture of both arises. Such mode is called HEM, hybrid electric-magnetic mode.

$$\begin{aligned} TE: H_t &= \frac{-\gamma}{\beta_c^2} \nabla H_z \\ TM: E_t &= \frac{-\gamma}{\beta_c^2} \nabla E_z \end{aligned} \quad (2-34)$$

Actually in a waveguide with the rectangular cross-section shown in Fig. 2, the equation is solved obtaining the following expression.

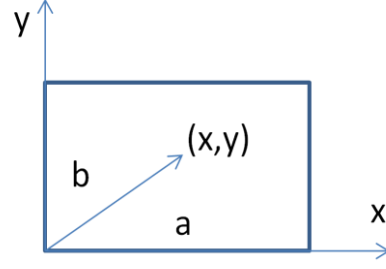


Fig. 2

$$H_z = A_{nm} \cos \frac{n\pi x}{a} \cos \frac{m\pi y}{b} e^{\mp j\beta z}$$

$$H_x = \pm j \frac{\beta_{nm}}{\beta_{c,nm}^2} A_{nm} \frac{n\pi}{a} \sin \frac{n\pi x}{a} \cos \frac{m\pi y}{b} e^{\mp j\beta z}$$

$$H_y = \pm j \frac{\beta_{nm}}{\beta_{c,nm}^2} A_{nm} \frac{m\pi}{b} \cos \frac{n\pi x}{a} \sin \frac{m\pi y}{b} e^{\mp j\beta z}$$

$$E_x = \pm Z_{h,nm} j \frac{\beta_{nm}}{\beta_{c,nm}^2} A_{nm} \frac{m\pi}{b} \cos \frac{n\pi x}{a} \sin \frac{m\pi y}{b} e^{\mp j\beta z}$$

$$E_y = -Z_{h,nm} j \frac{\beta_{nm}}{\beta_{c,nm}^2} A_{nm} \frac{n\pi}{a} \sin \frac{n\pi x}{a} \cos \frac{m\pi y}{b} e^{\mp j\beta z}$$

where

$$Z_{h,nm} = \frac{\beta_0}{\beta_{nm}} Z_0 = \frac{\lambda_g}{\lambda_0} Z_0$$

The actual field pattern can be calculated by many softwares. Some of very basic ones are shown in the Waveguide Handbook<sup>6</sup>.

Typical field pattern in a rectangular waveguide  
(Copied from Waveguide Handbook<sup>6</sup>)

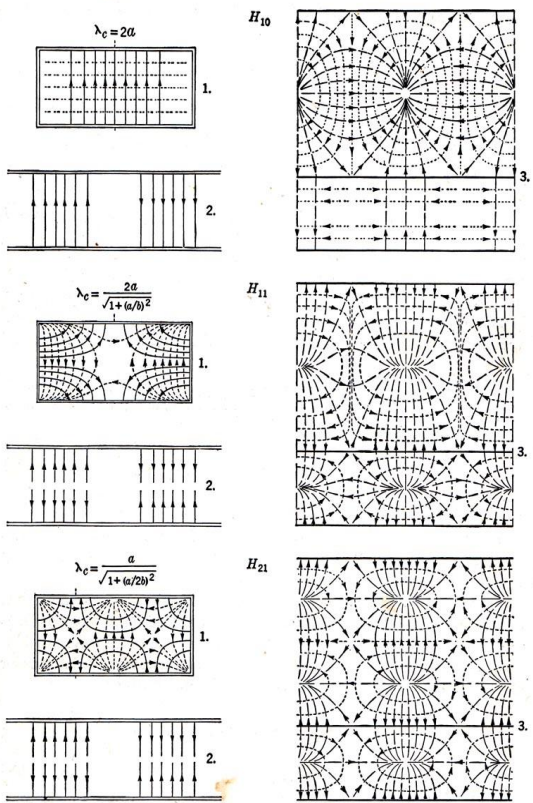


FIG. 2-3.—Field distribution for *H*-modes in rectangular waveguide.  
1. Cross-sectional view  
2. Longitudinal view  
3. Surface view

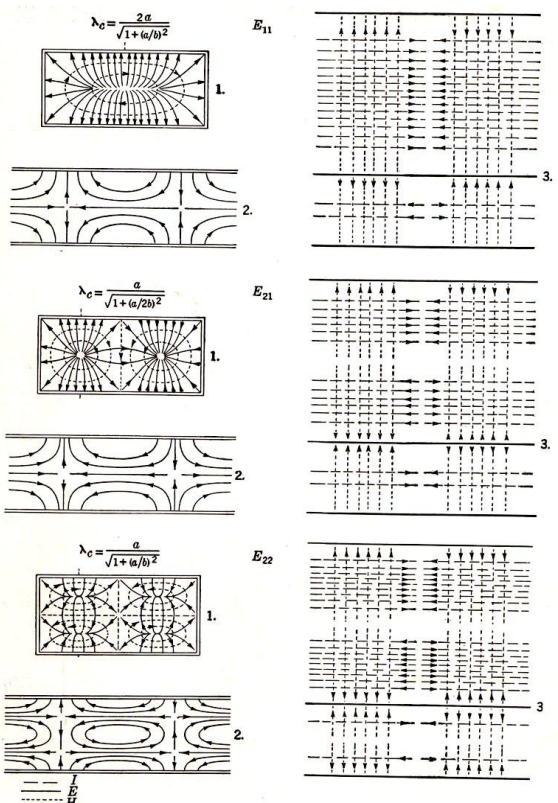


FIG. 2-2.—Field distribution for *E*-modes in rectangular guides.  
1. Cross-sectional view  
2. Longitudinal view  
3. Surface view

TM (E) mode

TE (H) mode

Fig. 3

If we solve the equation in the cylindrical coordinates, the solution of the TM modes become as the following.

$$E_r = -j \frac{\beta_m}{\beta_c} \cos(m\theta) J'_m(\beta_c r) e^{-j\beta z}$$

$$E_\theta = j \frac{m\beta_m}{\beta_c^2} \sin(m\theta) \frac{1}{r} J_m(\beta_c r) e^{-j\beta z}$$

$$E_z = \cos(m\theta) J_m(\beta_c r) e^{-j\beta z}$$

$$H_r = -j \frac{m\omega\epsilon}{\beta_c^2} \sin(m\theta) \frac{1}{r} J_m(\beta_c r) e^{-j\beta z}$$

$$H_\theta = -j \frac{\omega\epsilon}{\beta_c} \cos(m\theta) J'_m(\beta_c r) e^{-j\beta z}$$

$$H_z = 0$$

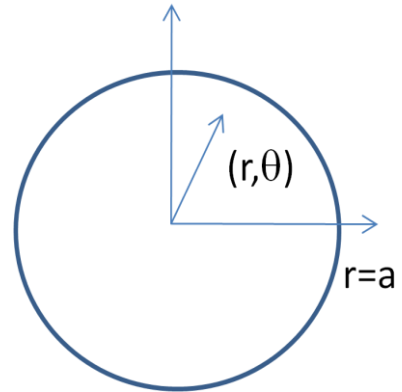


Fig. 4

The expression of TE modes is similar.

Typical pattern of those modes copied from Waveguide Handbook<sup>6</sup> are shown in the next page.



Typical field pattern in a cylindrical waveguide  
(Copied from Waveguide Handbook<sup>6</sup>)

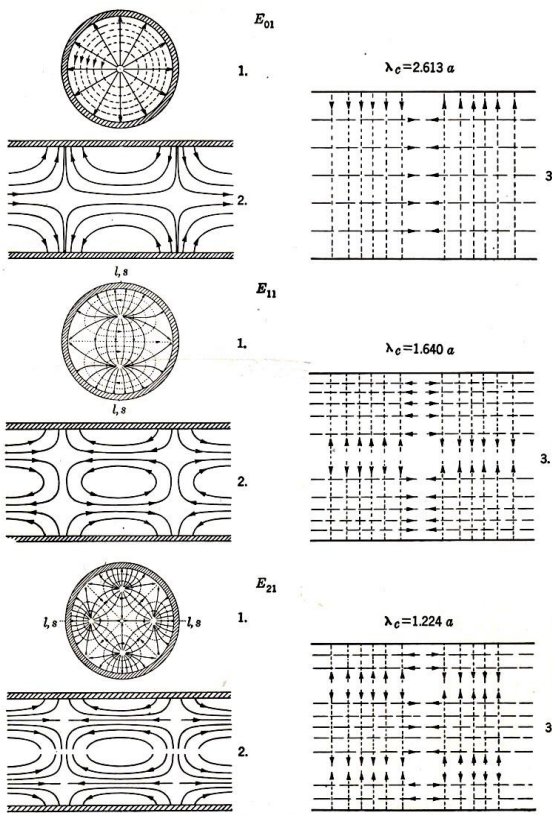


FIG. 2-5.—Field distribution for  $E$ -modes in circular waveguide.  
1. Cross-sectional view  
2. Longitudinal view through plane  $l-l$   
3. Surface view from  $s-s$

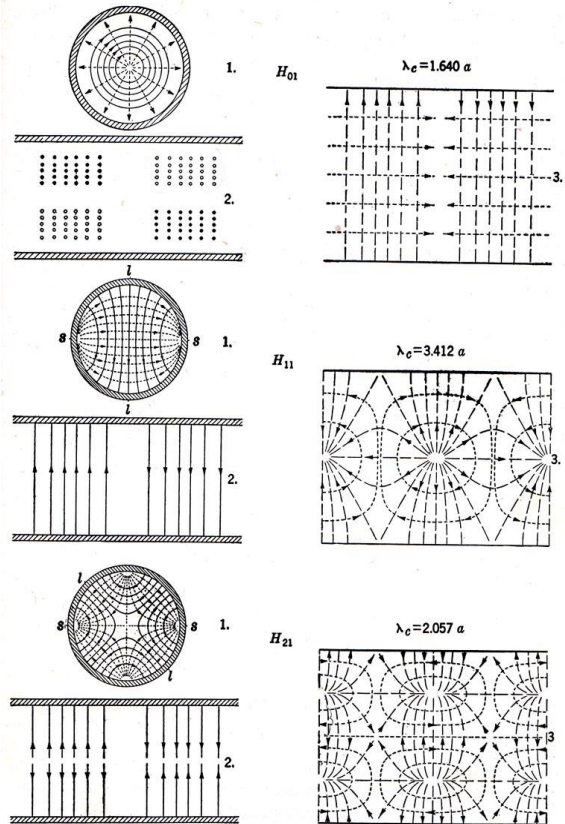


FIG. 2-6.—Field distribution for  $H$ -modes in circular waveguide.  
1. Cross-sectional view  
2. Longitudinal view through plane  $l-l$   
3. Surface view from  $s-s$

TM (E) mode

TE (H) mode

Fig. 5

Let us suppose loss-free transmission line. The propagation constant is expressed as

$$\gamma^2 = \beta_c^2 - \omega^2 \epsilon\mu = -\beta_z^2$$

where  $\beta_z$  is real if  $\omega > \omega_c$ . This dispersion relation is plotted in the right figure.

Here the wave propagates as

$$e^{j(\omega t - \beta_z z)}$$

and the dispersion is shown in the green curve. If the frequency  $\omega$  is at the red line, the phase velocity, pink line, becomes larger than light velocity, blue line, and no net acceleration is realized.

Dispersion diagram

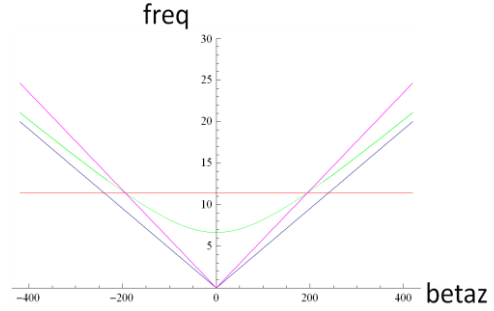


Fig. 6

Actually the most important mode for the acceleration, TM<sub>01</sub> mode, is expressed as

$$\begin{aligned} E_z &= E_0 J_0(\beta_c r) e^{j(\omega t - \beta_z z)} \\ E_r &= j E_0 Z_0 (1 - (\omega_c / \omega)^2) J_1(\beta_c r) e^{j(\omega t - \beta_z z)} \\ H_\theta &= j E_0 J_1(\beta_c r) e^{j(\omega t - \beta_z z)} \end{aligned}$$

### 2.3 Wave propagation in a periodically loaded waveguide

In order to make the net acceleration along a long line, it is needed to reduce the phase velocity. This is accomplished by introducing a small periodic perturbation along the line. The perturbation is called as “loading.”

If  $d$  is set as a half wavelength, then the reflections from each obstacle add coherently, making large reflection, and it results in a stop band in the dispersion. This occurs with harmonics  $\beta_z = 2\pi/d$  in the dispersion diagram.

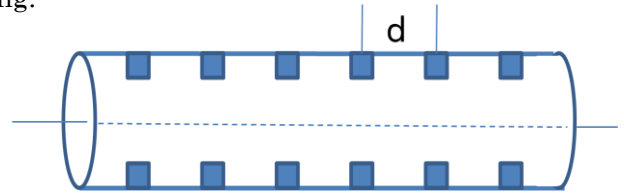


Fig. 7

From Floquet’s theorem in periodically loaded waveguide, the z-component of the electric field is expressed as

$$E_z = \sum_{n=-\infty}^{n=\infty} a_n J_0(k_{r_n} r) e^{j(\omega t - \beta_n z)}$$

where

$$\beta_n = \beta_0 + 2\pi n / d$$

$$k_{r_n}^2 = k^2 - \beta_n^2$$

Dispersion diagram

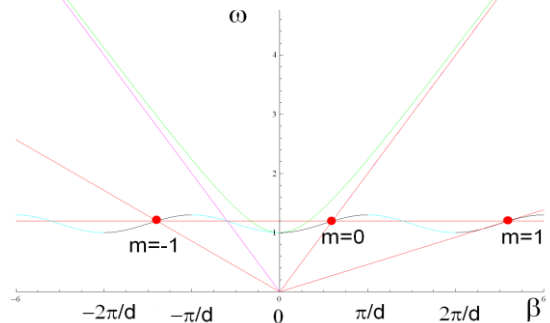


Fig. 8

Now it can be tuned to adjust the phase velocity to light velocity as shown with red dot in Fig. 8. Now with excitation at the frequency  $\omega$ , there are infinite number of modes, shown with red dots in the figure. Each point represent the space harmonics with numbering  $m$ . When we consider the acceleration of the particle with its velocity  $\beta=1$ , only  $m=0$  space harmonics contribute to the net acceleration for a long distance.

Up to here, we have seen the propagation of microwave mode along a waveguide. As the perturbation becomes large, the microwave system varies its nature as shown from top to bottom of Fig. 9. It is more practical to describe the heavily loaded system with isolated cavities with slight coupling through the aperture on the beam axis rather than describing the system from perturbation of propagation of mode in a uniform waveguide. This idea is shown in the same figure but seen from bottom to top as the coupling between cavities increases. In these cases, it is more practical to describe the system in a coupled chain of cavities.

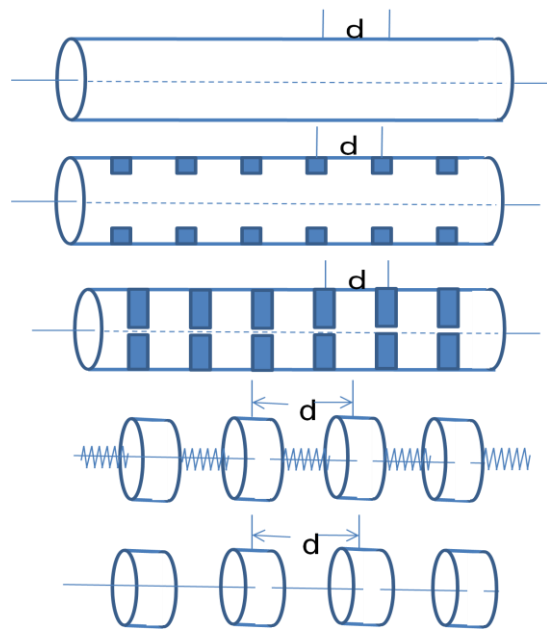


Fig. 9

In order to analyze the acceleration from the fundamental acceleration point of view, let us analyze one cavity system in the following chapter and study how the acceleration is analyzed.

### 3. Cavity as a unit of acceleration

#### 3.1 Inside a cavity

All the cavities should be operated synchronously with beam for the continuous acceleration along a long distance. For this purpose, the cavities are driven by externally phase-controlled RF source system or with automatic phasing among cavities with a resonant behavior as a whole. The former needs many input circuits and also care should be taken to control the relative phase among cavities. This requirement is tedious and also the space factor for the effective acceleration length decreases as the connection region need some space and also the input circuit need some extra space without acceleration. Therefore, it is preferable to resonantly excite as many cavities as possible in a single resonant mode as a whole.

There are two ways to resonantly excite the whole cavity system, travelling wave (TW) propagation through the structure and standing wave (SW) storage in a cavity, both are composed of as many accelerating cells as possible. In both cases, there are several important cavity parameters, or structure parameters, relevant to the acceleration; the resonant frequency, the shunt impedance  $R/Q$  which measures how the accelerating field is focused on beam axis w.r.t. stored energy in a cell, the shunt impedance  $R$  which represent the acceleration w.r.t. power loss into the cavity wall due to the storage of the acceleration mode, the loss factor  $k_L$ , which is directly related to  $R/Q$  and measures the energy left in the empty cavity after a bunch passes the cavity. In the following sections, we review these parameters of a single accelerating cell as a basic parameterization of the cavity.

#### 3.2 Frequency

The resonant frequency of the electric resonant circuit is described as

$$Freq = \frac{1}{2\pi\sqrt{LC}} \quad , \quad (3-1)$$

where  $L$  and  $C$  are the inductance and capacitance of the circuit. The resonant frequency of the cavity can be described in the same form as long as the parametrization of the cavity field is done by using the equivalent circuit parameters. When the cavity surface makes a positive bump in the high magnetic field area, the inductance will decrease because the magnetic field volume becomes less while the strength of the field is kept. This perturbation makes the resonant frequency of the circuit higher. On the other hand, when the positive bump appears on the electrodes which terminate the electric field, the capacitance becomes larger and it makes the resonant frequency lower. The quantitative analysis on such perturbation was analyzed by Slater<sup>7</sup> and shown as below.

$$\frac{\omega^2 - \omega_0^2}{\omega_0^2} = \int_{\delta V} (H^2 - E^2) dV \quad (3-2)$$

$$\int_{Cavity} H^2 dV \equiv 1, \quad \int_{Cavity} E^2 dV \equiv 1$$

This is called as the Slater's perturbation theorem. Many of the cavity tuning procedures are done following this theorem. An example in the normal conducting cavity cell is shown in Fig. 10. Four

Dimple tuning in NCC cavity

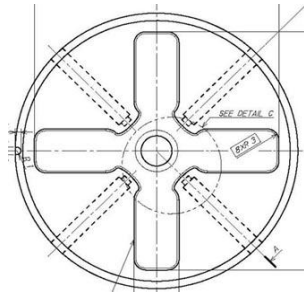


Fig. 10

Tuning of SCC cavity by deforming

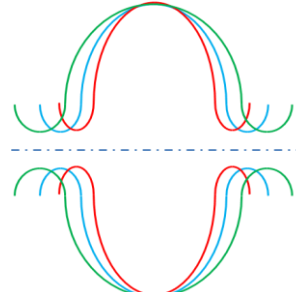


Fig. 11

dimples (positive for higher frequency and negative for lower frequency) are formed through push/pull mechanism inserting from outside targeting at four thin areas. Another example is shown in Fig. 11 in the superconducting cavity case. The sky blue shape is the nominal shape, while the green shape is formed by pulling the cavity at the iris region so that the frequency goes up, and the red shape is formed by pushing the iris area to reduce the frequency of the cell. Such deformation is possible because the cavity comprises of thin niobium plate. However, this tuning method may perturb the adjacent cell shape and the frequency so that the mechanical property related to the tuning of cell  $n$  should be carefully understood including the effect to the nearest neighbor cells.

### 3.3 Acceleration related parameters

The very basic parameters related to the acceleration in an accelerator cell are described as follows.

|   |   |       |
|---|---|-------|
| $V = \int E_z(z, t) dz$ $R \equiv \frac{V^2}{P_c}$ $R/Q \equiv \frac{V^2}{2\omega U}$ $Q \equiv \frac{\omega U}{P_c} = \frac{G}{R_s}$ | $E_{acc} = V/L$ $R/L = \frac{E_{acc}^2}{(P_c/L)}$ $(R/L)/Q = \frac{E_{acc}^2}{(P_c/L)}$ $Q = \frac{\omega(U/L)}{(P_c/L)}$ | (3-3) |
|---|---|-------|

Here the left parameters in a blue box are those of a cell, or those of a cavity, while the right parameters in a red box are the parameters in the units per unit length. The  $L$  stands for cavity length,  $V$  the voltage of acceleration in the cavity,  $E_{acc}$  the accelerating gradient over the cell,  $R$  shunt impedance,  $R/Q$  the impedance and  $Q$  the  $Q$  value of the cell. The wall loss in the cavity inner surface,  $P_c$ , and the stored energy in the cavity,  $U$ , are described as

$$P_c = \frac{R_s}{2} \int |H^2| dS \quad R_s = \sqrt{\frac{\omega\mu}{2\sigma}} \quad (3-4)$$

$$U = \frac{\mu}{2} \int |H^2| dV = \frac{\varepsilon}{2} \int |E^2| dV \quad ,$$

and the geometrical factor  $G$ , which is commonly used for SCC cavity discussion, is defined as

$$G \equiv \omega\mu \frac{\int |H^2| dV}{\int |H^2| dS} \quad (3-5)$$

where this factor uniquely determined by the cell shape.

### 3.4 $R/Q$

How to focus the  $E_z$  field along the beam axis is an important parameters of efficient acceleration. This is simply because the  $R/Q$  definition,

$$R/Q \equiv \frac{V^2}{2\omega U} \quad , \quad (3-6)$$

which is the ratio of field squared per stored energy over the cavity.

In order to increase  $R/Q$ , the smaller beam aperture is important but there is of course a limit due to the finite aperture needed for the coupling between cells in addition to the enough beam stay clear aperture requiring the beam pipe radius. If we can make the cell-to-cell coupling by some other mean than beam hole aperture coupling, such as in the side coupled structure, the cell design with nose cone as shown in Fig. 12 is effective to increase  $R/Q$ .

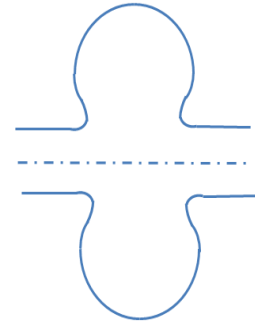


Fig. 12

For the ILC SCC cavity design, the smooth surface is required for making it possible to be polished with liquid inside and finally to be rinsed in high pressure water treatment. In this aim, it is difficult to put a nose cone. However, an idea came<sup>8</sup> out to make one side of the cavity be equipped with nose cone to increase  $R/Q$  while the other side to be without to make it possible to treat without making upside down. Otherwise, the nose cone is difficult for SCC cavity design. The only way to increase  $R/Q$  is to reduce the beam hole aperture and the limit from beam dynamics point of view determine the radius.

In the disk loaded structure, DLS, there is few parameters to increase R/Q instead of reducing the beam aperture. However, it is possible to increase R/Q a little by shaping the cavity with the similar geometry as the nose cone.

It is to be noted that the choke mode cavity, DLS being designed for heavily damping higher modes, needs the stored energy at the choke to establish the accelerating mode field inside the acceleration cell so that some extra stored energy is needed and this makes R/Q smaller by typically several percents.

Another key parameter, loss parameter  $k_L$ , is directly related to R/Q. It is expressed as

$$k_L = \frac{\omega R}{4Q} \quad (3-7)$$

The energy left in a mode after a bunch of charge  $q$  passes the cavity is expressed as

$$U_m = k_{L,m} q^2 \quad (3-8)$$

where  $m$  is the mode number and  $U_m$  the energy left in the mode  $m$ . This means that the larger R/Q makes the stored energy large left behind the bunch passage. Therefore, the cavity with higher R/Q is susceptible to the change of the accelerating mode, transverse kick if the mode is transverse mode, and may suffer from the heating problem because the total energy left behind is the sum of all  $U_m$ , especially the left field is resonantly built up. This is very critical in the application to the cavity for the ring because of many-times passage of the beam, while the cavity for linac only needs to be within a limit for finite number of bunches in a train. Therefore for the linac application, R/Q is usually designed to be as high as possible.

There is another important idea, transit time factor, related to the R/Q. The time varying field changes its amplitude while beam passes the cavity. The acceleration field behaves as

$$E_z(z, t) = E_0 e^{j\omega t} \quad (3-9)$$

and the values without taking the time variation into account are defined as

$$R_{un} = \frac{V_0^2}{P} \quad \text{with} \quad V_0 = \int_{-L/2}^{L/2} E(z, t=0) dz \quad (3-10)$$

where  $V_0$  is the voltage acquired by the beam of infinite velocity. Let us consider the  $TM_{010}$  mode in a pillbox cavity. Since the acceleration field is expressed as

$$E_z(z, t) = E_0 \text{Cos}(\omega t), \quad z = ct \quad (3-11)$$

the voltage the beam acquires is written as

$$V(L) = \int_{-L/2}^{L/2} (E_0 \text{Cos} \omega t) d(ct) = \frac{2c E_0}{\omega} \text{Sin}\left(\frac{\omega L}{2c}\right) \quad (3-12)$$

and the transit time factor defined as

$$T \equiv V(L)/V_0 \quad (3-13)$$

and it becomes

$$T = \frac{2c}{\omega L} \text{Sin}\left(\frac{\omega L}{2c}\right) = \frac{\text{Sin}(x)}{x}, \text{ where } x = \frac{\omega L}{2c} \quad (3-14)$$

This Sin(x)/x functional behavior of transit time factor is plotted in Fig. 13. In the  $\pi$ -mode cavity as ILC SCC cavity,

$$c \frac{1}{2f} = L$$

The x becomes  $\pi/2$  and the transit time factor becomes 0.64.

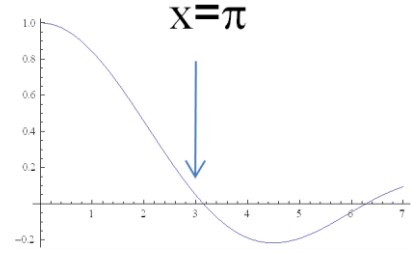


Fig. 13

### 3.5 Surface loss and Q value

The Q value of a cavity, which we call the intrinsic Q value and names as  $Q_0$ , is a measure of the voltage established in the cavity for a given input power level. It is usually better to be as high as possible. It is simply written as

$$Q = \frac{G}{R_s}$$

where the  $G$  and  $R_s$  are, as described before, the geometrical factor and the surface resistance, respectively. The former is determined completely by the geometry of the cavity, which is proportional to the volume integral of the magnetic field squared divided by the surface integral of the magnetic field squared.

The  $R_s$  is determined by the choice of material and operation temperature. For the ILC case with a superconducting material of Niobium at 2K, one of the main contributions to the surface resistance can be calculated from a simple formula<sup>9</sup> as

$$R_{BCS}(\Omega) = 2 \times 10^{-4} \frac{1}{T} \left(\frac{f}{1.5}\right)^2 e^{-\frac{17.67}{T}}, \text{ where } f(\text{GHz}), T(^{\circ}\text{K})$$

This is the resistance only from BCS resistance. It becomes of the order of 10n $\Omega$  at 2K. It is noted that the higher frequency makes the BCS resistance higher in a quadratic manner and this behavior makes it difficult to cite the higher frequency in ILC where very long pulse length makes the power needed for cryogenic cooling becomes huge. In reality, the actual surface resistance is the addition of other effect on this BCS one and how to reduce the other effect is one of the key issues for the ILC development, especially when targeting for the higher gradient operation. It is because the low Q leads again to the higher cryogenic cooling power.

On the other hand in normal conducting material such as copper, the surface resistance is as eq. (3-4) and it becomes about 28m $\Omega$  at room temperature for copper. This value is 6 orders of



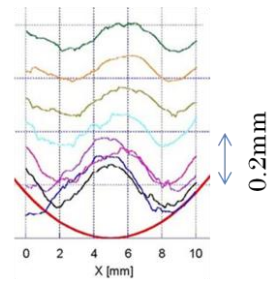
magnitude larger than Nb at 2K! It is to be noted that the power loss is large and also it sits within a thin layer, a few times of the skin depth with exponential decay. Then only the surface is heated up during the pulse because the thermal diffusion in copper is only about 10 microns order during a few hundred nano second pulse width. This results in the pulse temperature rise on surface and may deteriorate the copper surface by fatigue through many-pulses during a long term operation.

From here we review how to increase Q value in a few cases to show the effort for high Q from geometry point of view. In the ILC SCC cavity starting from TESLA shape cavity, the low-loss cavity is designed by reducing the peak magnetic field at the outer region of the cell by uniformly distribute the magnetic field which is needed for establishing the  $E_z$  field on axis. On the other hand, in the DLS structure in the NCC structure case, the cell geometry can be tuned to make it as close as sphere so that the magnetic field distribution is made more uniform comparing to the usual DLS where the cell shape is essentially a pillbox with right angle geometry rather than the smooth shape in near spherical shape. In the heavily damped structure with choke structure, some power loss is inevitable in the choke and it loses several percent of power there and it makes the Q value lower. In a heavily damped structure with the damping waveguide coupled with the cell wall, such as shown in Fig. 10, the magnetic field at the opening edge is enhanced and small opening aperture is needed to keep Q high.

### 3.6 Cares on local field

It is preferable in many cases to suppress the enhancement of the local electric field or local magnetic field. The excessive electric field sometimes causes the field emissions and breakdowns. On the other hand, the excessive magnetic field results in pulse surface temperature rise in NCC or quenching in SCC cavity. We design the cavities with suppressing the ratio of these local field w.r.t. the accelerating gradient,  $E_p/E_{acc}$  and  $H_p/E_{acc}$ .

Firstly these ratio should be kept small from cavity global geometry. In addition, the local enhancement due to fabrication should be minimized. Examples are such as the bumps over electron beam welding line for ILC SCC cavity as shown in Fig. 14. The figure shows the measured example of the contour over the EBW line of the equator junction. Another example is the smooth geometry design and cares of less burrs and steep tangential discontinuities over the opening area in various places in an actual DLS structure as shown in Fig. 15. The magnetic field enhancement at the opening edge is estimated by 2D field solving code. The simulated field pattern and the result of magnetic field enhancement is plotted as function of radius at the edge in Fig. 16.



Bump over EBW line

Fig. 14

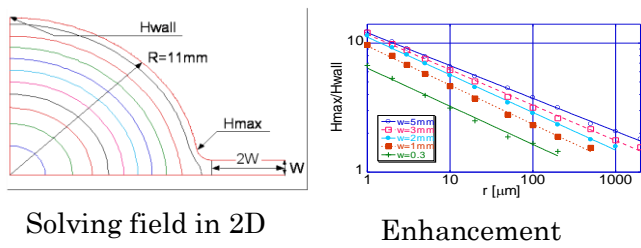


Fig. 16

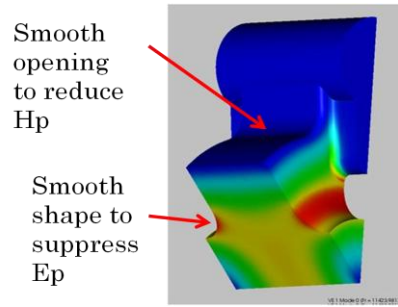
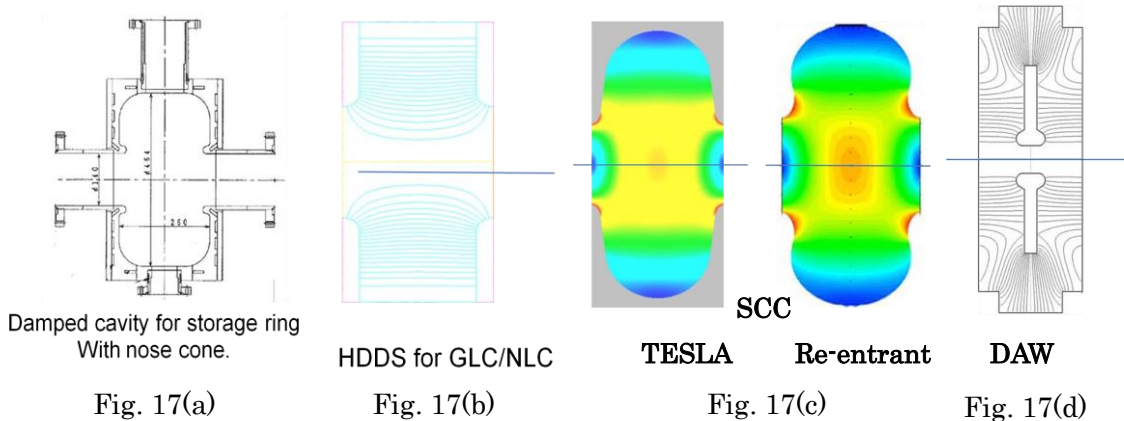


Fig. 15 Es field distribution.

In Fig. 17 below are shown various cavity shapes as a review of some typical cavity shapes. The left figure (a) shows a single cavity for storage ring with large R/Q but no need to couple between cells. Fig. 17 (b) is an example of DLS of TW linac, where the field plotted is that of  $\pi$ -mode while the actual mode is TW  $5\pi/6$  mode, the modal field pattern not simple to plot. Two of Fig. 17 (c) are SCC cavities related to ILC. Right one is re-entrant with nose cone, while left one is the TESLA one. The main difference between them is at the slope to the iris. The last one (d) shows disk-and-washer DAW cavity, showing the possibility to use other mode than pillbox  $TM_{010}$  mode origin. Actually the mode in DAW is similar to  $TM_{020}$  and  $TM_{011}$  in a pillbox. The shunt impedance of this cavity is high if the design for support of washer does not deteriorate the field pattern much. However, the adoption of higher mode as the accelerating mode may makes the system complex than those based on the lowest frequency  $TM_{010}$  mode. The fabrication is also complex so that for the LC application to date, only the choices of (b) and (c) are thought to be reasonable.



Damped cavity for storage ring  
With nose cone.

Fig. 17(a)

HDDS for GLC/NLC

Fig. 17(b)

TESLA

Re-entrant

DAW

Fig. 17(c)

Fig. 17(d)

## 4. Coupled cavity system in a SW regime

### 4.1 Coupled resonator model

Each accelerator cell, cavity, has its internal freedom. This can be analyzed with eigen modes of the cavity. The excited accelerating mode couples to beam to make acceleration and deceleration and the beam excited modes transversely kick the other beam and so on. These can be analyzed with the eigen modes of the cavity. However, the total system is, as stated before, a coupled resonator system. This system can be treated as a system with weakly coupled resonators. This is equivalent mathematically to that of the system with mechanically coupled resonators or that of electrically coupled resonators. The following discussion follows basically the analysis by Knapp et al.<sup>10</sup>

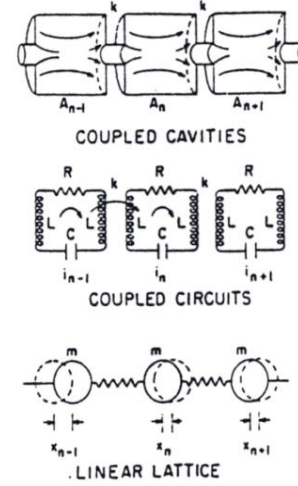


Fig. 18

Let us focus on accelerating mode. In this single mode case, we can describe the system as follows:

$$\begin{aligned}
 I_0 &= X_0 \left(1 + \frac{\omega_0}{j\omega Q} - \frac{\omega_0^2}{\omega^2}\right) + k X_1 \\
 I_n &= X_n \left(1 + \frac{\omega_0}{j\omega Q} - \frac{\omega_0^2}{\omega^2}\right) + \frac{k}{2} (X_{n-1} + X_{n+1}) \\
 I_N &= X_N \left(1 + \frac{\omega_0}{j\omega Q} - \frac{\omega_0^2}{\omega^2}\right) + k X_{N-1}
 \end{aligned} \tag{4-1}$$

where the parameters are defined as

$$\begin{aligned}
 \omega_0^{-2} &= 2LC \\
 X_n &= \sqrt{2L} i_n \\
 Q &= 2\omega_0 L/R
 \end{aligned} \tag{4-2}$$

This set of equation has a solution in a loss free case,  $Q \gg 1$ , as below.

$$X_n^q = \text{const} \cos\left(\frac{\pi q n}{N}\right) e^{j\omega_q t} \quad \text{with} \quad \omega_q^2 = \frac{\omega_0^2}{1 + k \cos\left(\frac{\pi q}{N}\right)} \tag{4-3}$$

The above gives  $q$ -th eigen frequency and  $q$ -th eigen mode at  $n$ -th cavity. In the SCC cavity with  $\pi$  phase advance per cell, this solution gives such dispersion (left) and the mode pattern (right) with red line as shown in Fig. 18. We also show here the blue curve

of the field pattern of  $\pi/9$  mode which is the lowest mode within the same passband as accelerating mode. By making the flat  $\pi$ -mode, accelerating mode, the 0-mode is perturbed at the end and is not flat pattern.

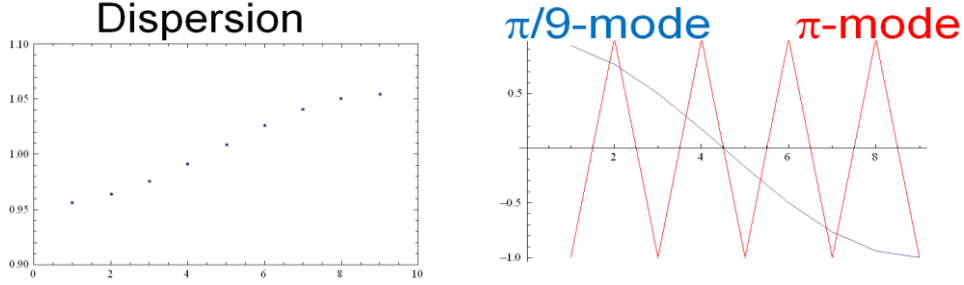


Fig. 18 9-cell SCC cavity. Left: dispersion and right: field pattern.

#### 4.2 Perturbation analysis

The set of equations is also written in the matrix form as below.

Matrix:

$$X \equiv \begin{bmatrix} X_0 \\ X_1 \\ \vdots \\ X_N \end{bmatrix}, M \equiv \begin{bmatrix} 1 & k & 0 & & 0 \\ k/2 & 1 & k/2 & 0 & 0 \\ & k/2 & 1 & k/2 & 0 \\ \bullet & \bullet & \bullet & \bullet & \bullet \\ 0 & & 0 & k/2 & 1 & k/2 \\ 0 & 0 & & 0 & k & 1 \end{bmatrix} \quad (4-4)$$

Equation:

$$M X - \left(\frac{\omega_0}{\omega}\right)^2 X = 0 \quad (4-5)$$

Solution vector:

$$X^q = \begin{bmatrix} 1 \\ \cos(\pi q / N) \\ \vdots \\ \cos(\pi q n / N) \\ \vdots \\ \cos \pi q \end{bmatrix} \quad (4-6)$$

When errors exist, the matrix equation becomes to the first order of errors as

$$M \delta X^q = \frac{\omega_0^2}{\omega_q^2} \delta X^q + \begin{bmatrix} \delta\left(\frac{\omega_{00}^2}{\omega_q^2}\right) & 0 & 0 & 0 \\ 0 & \delta\left(\frac{\omega_{01}^2}{\omega_q^2}\right) & 0 & 0 \\ \bullet & \bullet & \bullet & 0 \\ 0 & 0 & 0 & \delta\left(\frac{\omega_{0N}^2}{\omega_q^2}\right) \end{bmatrix} X^q \quad (4-7)$$

Solving this equation with the error assumption, we can analyze the system stability against frequency errors. For the  $\pi$ -mode,

$$\delta X_n^\pi / X_n^\pi = \sum_{p=1}^N \tilde{\varepsilon}_p (1-k) \text{Cos} \pi \frac{pn}{N} / k (1 - \text{Cos} \frac{\pi p}{N}) \quad (4-8)$$

and for the  $\pi/2$  mode,

$$\delta X_n^{\pi/2} / X_n^{\pi/2} = \frac{1}{k} \sum_{p=1}^N \tilde{\varepsilon}_p \left( \text{Sin} \frac{\pi pn}{N} \text{Sin} \frac{\pi n}{2} / \text{Sin} \frac{\pi p}{N} \right) \quad , \quad (4-9)$$

where the  $\tilde{\varepsilon}_p$  is Fourier component of frequency errors of  $\text{Cos}(\pi pn/N)$  where  $p$  is the mode number. It is noted that both perturbation scales as  $1/k$ , inversely proportional to the coupling. This means the larger coupling makes the system more stable. From the denominator, we see that the  $\pi$ -mode becomes unstable for larger number of cells, for the case with large  $N$ . This is because the energy exchange between cells at  $\pi$ -mode is not very effective because the group velocity is zero at  $\pi$ -mode so that there needs other modes than  $\pi$ -mode to recover the frequency errors by communicating among cells. Actually the perturbed field scales as  $N^2$ , while that of  $\pi/2$  mode linearly to  $N$ . Therefore, the  $\pi$ -mode operation cannot be designed for larger  $N$ , the degree of which depends on the frequency error amount.

#### 4.3 Choice of acceleration mode

In the right figure, we show various modes with phase advance per cell as the naming of such modes. The zero mode is the most simple mode but no net acceleration. The next  $\pi/2$  mode is stable but half of the cells do not contribute to the acceleration. The  $2\pi/3$  mode is usually used in most of the DLS linac because the shunt impedance of the mode in TW gives broad maximum as function of phase advance for the typical DLS structures<sup>11</sup>. The  $\pi$  mode is the most typical case in SW linacs. This mode is weak against perturbation but simple periodic chain makes the acceleration for every cell with high shunt impedance. Therefore, the ILC SCC cavity adopted this mode. The number of cell is limited to 9 cell. In order to increase the number of cells effectively, other idea such as the super-structure<sup>12</sup> should be applied.

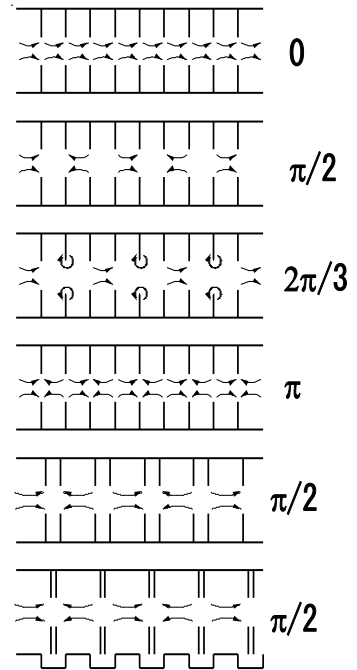


Fig. 19

The LC linac has not applied other  $\pi/2$  mode such as those shown in the last two cases. The choice of Fig. 17(d) is also an attractive choice of  $\pi/2$  mode. In

these designs, the high shunt impedance and the stable mode along a long cavity is realized at the same time but the complex tuning procedures (the adjustment of the accelerating mode and the so-called coupling mode) is necessary to realize the stable accelerating mode. In addition the complexity of such geometries makes it costly. Therefore, unless the choice of these structures is inevitable from technical point of view, the LC linac will not take the  $\pi/2$  mode design.

#### 4.4 Some analysis of nine cell SCC cavity

The cell-to-cell coupling constant of ILC cavity  $\kappa \sim 2\%$ . The dispersion relation of the mode with the phase advance per cell  $\phi$  is described as

$$F(\phi) \propto \frac{F_0}{\sqrt{1 + \kappa \cos(\phi)}} \quad , \quad (4-10)$$

so that the band width becomes

$$BW \approx \kappa F_0 \approx 26 \text{ MHz}$$

It is usually important to know the separation between acceleration mode and the nearest neighbor mode, here  $8\pi/9$  mode. For the ILC SCC cavity case, it becomes,

$$F_\pi - F_{8\pi/9} \approx 0.06 BW \approx 0.15 \text{ MHz}$$

Since it uses  $\pi$  mode, the shunt impedance of the whole 9-cell cavity becomes simply 9 times of that of the single cell.

In such SCC cavity as ILC one, the excessive field in any of the 9 cells may cause the quenching at the cell and the quenching usually expands quickly to the whole cavity. Therefore, the flat  $\pi$  mode operation is one of the key issues to make the acceleration gradient high. The field flatness of the SCC cavity is deteriorated by frequency errors among the cells in the cavity. Some error comes from the fabrication imperfection such as from the EP process, and some from the dynamic process called as ‘Lorentz force detuning’, which is the result of the Maxwell’s stress on the cavity surface.

A simple analysis on these errors and field flatness can be performed as described in the previous section. The measured field errors  $\delta x$  is used for estimation of cell frequency errors. This error will be corrected by mechanical deformation as described in section 3.2 and the field flatness is measured again. This iteration process is applied until good flatness is realized. The iteration is shown in Fig. 20.

$$\begin{aligned} M_0 \cdot x_0 &= \lambda_0 x_0 \\ (M_0 + \delta) \cdot (x_0 + \delta x) &= (\lambda_0 + \delta \lambda) (x_0 + \delta x) \\ \therefore \delta \cdot x_0 + M_0 \cdot \delta x &= \delta \lambda \cdot x_0 + \lambda_0 \cdot \delta x \end{aligned} \quad (4-11)$$

because  $\delta\lambda/\lambda_0 \ll |\delta x|/x_0$  (4-12)  
then  $\delta \cdot x_0 = (\lambda_0 - M_0) \cdot \delta x$

Because we know design values,  $x_0$ ,  $\lambda_0$ ,  $M_0$  and measured error of field  $\delta x$ , then we obtain the error in frequency  $\delta$

$$\delta = 2 \cdot (\delta\omega / \omega_0)$$

from the above matrix equation (4-12). The cycle of the iteration is shown in Fig. 20. Since the process suffer from error in tuning, this cycle should usually be iterated.

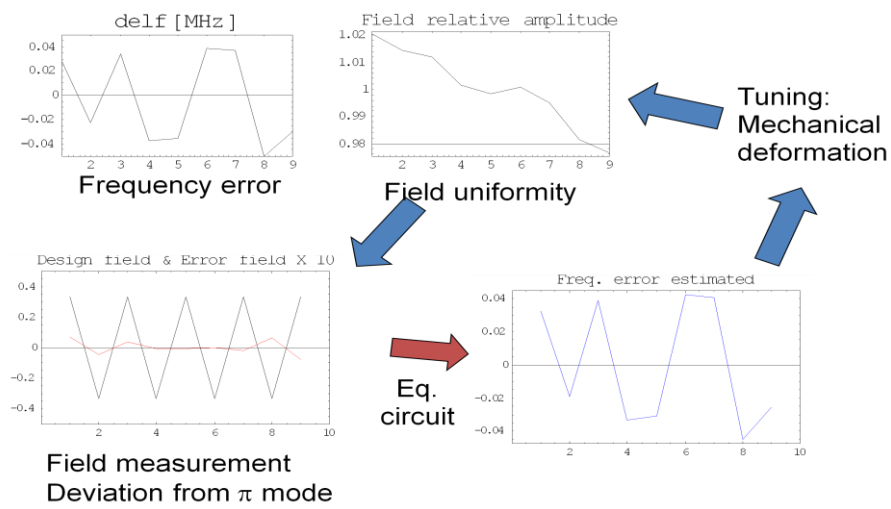


Fig. 20

## 5. Pillbox as a simple base to represent practical cavities

### 5.1 Pillbox cavity expression

It is easy to make a cylindrical cavity because of easy fabrication, mechanical stability, easy to establish symmetry and so on. Therefore, many cavities for the accelerator are close to the pillbox cavity to some extent.

In a cylindrical waveguide, there are two propagation modes exist,

$$e^{i(\omega t - \beta)z} \quad \text{and} \quad e^{i(\omega t + \beta)z} \quad (5-1)$$

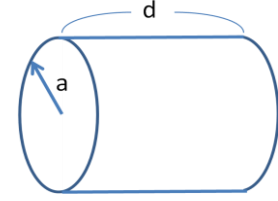


Fig. 21

but when two ends are closed with metal to make a pillbox, the boundary condition at the two ends makes various

parameters determined with two counter-directed wave to be superposed. In the TM modes, the field is described as below.

$$\begin{aligned} E_r &= -\frac{\beta_z}{K_c} \cos(m\theta) J'_m(K_c r) \sin(\beta_z z) \\ E_\theta &= \frac{m\beta_z}{K_c^2} \sin(m\theta) \frac{1}{r} J_m(K_c r) \sin(\beta_z z) \\ E_z &= \cos(m\theta) J_m(K_c r) \cos(\beta_z z) \end{aligned} \quad (5-2)$$

$$H_r = -j \frac{m\omega \epsilon}{K_c^2} \sin(m\theta) \frac{1}{r} J_m(K_c r) \cos(\beta_z z)$$

$$H_\theta = -j \frac{\omega \epsilon}{K_c} \cos(m\theta) J'_m(K_c r) \cos(\beta_z z)$$

$$H_z = 0$$

$$\text{where } K_c = \rho_{mn}/a, \quad \beta_z = l\pi/d$$

These are called standing wave, SW, field. There are three suffices,  $m$  stands for the rotational symmetry,  $n$  the numbering of the nodes of Bessel's function identifying the modal number in the radial direction and  $l$  the numbering of nodes in  $z$ -direction. We call the mode as  $TM_{mnl}$ . The TE modes are described in the similar manner. In Fig. 22 are shown three cases of the radial variation. Red line is  $E_z$  field, while blue  $H_\phi$  field.

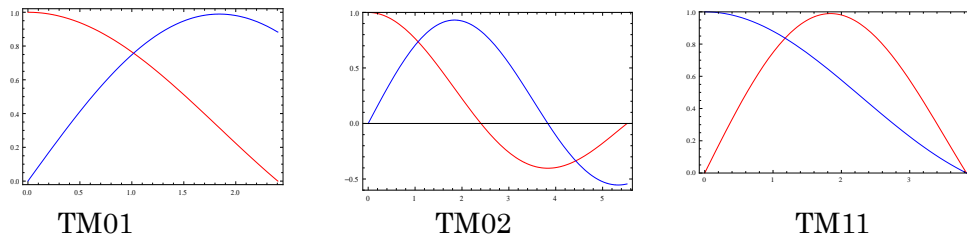


Fig. 22 Red =  $E_z$  and Blue =  $H_\phi$ .



From these field patterns, we understand that the TM01 mode is usually used for the acceleration with zero magnetic field on axis. The TM02 mode stores more energy with the same acceleration field so that if lower R/Q is needed, we can use this mode. The third one is TM11 with the rotational variation. This mode represent a dipole field, where the magnetic field on axis exists and the Ez field change sign when crosses the beam axis, meaning that the coupling of this mode to the beam is larger in large offset of the beam.

The frequency of the modes are calculated from

$$\left(\frac{\omega_{mnl}}{c}\right)^2 = \left(\frac{\rho_{mn}}{a}\right)^2 + \left(\frac{l\pi}{d}\right)^2 \quad (5-3)$$

The frequencies are plotted as in Fig. 23 for all of the TM modes. From this pattern, we understand that the modal density increases as frequency goes up.

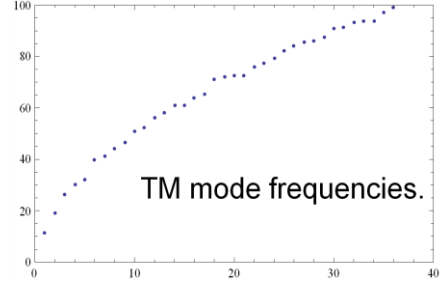


Fig. 23

## 5.2 Q value of pillbox cavity

The Q value-related parameters are defined as below.

$$U = \frac{\mu}{2} \int |H|^2 dV = \frac{\varepsilon}{2} \int |E|^2 dV, \quad P = \frac{R_s}{2} \int |H|^2 dS, \quad Q = \frac{\omega U}{P} \quad (5-4)$$

The integration is performed as

$$\begin{aligned} \int |H|^2 dV &= \int (H_r^2 + H_\theta^2) r dr d\theta dz \\ &= A d \int [H_r^2(z=0) + H_\theta^2(z=0)] r dr d\theta \\ &\text{where } A=1 \text{ for } \ell=0 \text{ and } A=1/2 \text{ for } \ell \neq 0 \end{aligned} \quad (5-5)$$

Then for  $m$  not equal to 0,

$$\begin{aligned} \int |H|^2 dV &= A \pi d \left(\frac{\omega \varepsilon}{K_c}\right)^2 \int \left[\left(\frac{m}{K_c r}\right)^2 J_m^2(K_c r) + J_m^2(K_c r)\right] r dr \\ &= A \pi d \left(\frac{\omega \varepsilon}{K_c}\right)^2 I(r=a) \\ &= A \pi d \left(\frac{\omega \varepsilon}{K_c}\right)^2 \frac{a^2}{2} J_m^2(\rho_{mn}) \end{aligned} \quad (5-6)$$

And similar result is obtained for  $m=0$ . Here we use the integration

$$\begin{aligned} I &\equiv \int \left[\left(\frac{m}{K_c r}\right)^2 J_m^2(K_c r) + J_m^2(K_c r)\right] r dr \\ &= \frac{r^2}{2} \left[ J_m^2(K_c r) + \frac{2}{K_c r} J_m'(K_c r) J_m(K_c r) + \left\{1 - \left(\frac{m}{K_c r}\right)^2\right\} J_m^2(K_c r) \right] \end{aligned} \quad (5-7)$$

Finally we get

$$\int |H|^2 dV = AB\pi d \left(\frac{\omega\mathcal{E}}{K_c}\right)^2 \frac{a^2}{2} J_m'^2(\rho_{mn}) \quad (5-8)$$

where  $B=2$  for  $m=0$  and  $B=1$  for  $m \neq 0$

On the other hand, the surface integral is performed as follows:

$$\begin{aligned} \int |H|^2 dS &= 2 \int [H_r^2(z=0) + H_\theta^2(z=0)] r dr d\theta + \int [H_\theta^2(r=a)] a d\theta dz \\ &= 2B\pi \left(\frac{\omega\mathcal{E}}{K_c}\right)^2 \frac{a^2}{2} J_m'^2(\rho_{nm}) + AB\pi d \left(\frac{\omega\mathcal{E}}{K_c}\right)^2 a J_m'^2(\rho_{nm}) \\ &= B\pi \left(\frac{\omega\mathcal{E}}{K_c}\right)^2 a(a+Ad) J_m'^2(\rho_{nm}) \end{aligned} \quad (5-9)$$

Collecting these integrals, we get for the TM mode

$$Q = \frac{1}{\delta_s} \frac{a}{1 + \frac{a}{Ad}}, \quad \text{where the skin depth is } \delta_s = \sqrt{\frac{2}{\sigma\omega\mu}}. \quad (5-10)$$

Similarly for the TE mode, we obtain

$$Q = \frac{1}{\delta_s} \frac{a[\rho_{mn}'^2 + (\frac{a}{d})^2 (\ell\pi)^2](\rho_{mn}'^2 - m^2)}{\rho_{mn}'^4 + 2(\frac{a}{d})^3 (\ell\pi\rho_{mn}')^2 + (\frac{a}{d})^2 (1 - \frac{2a}{d})(\ell\pi m)^2} \quad (5-11)$$

### 5.3 R/Q value of a pillbox cavity

Acceleration in a pillbox cavity is calculated as

$$\begin{aligned} E_{acc} &= \frac{1}{d} \int_{-d/2c}^{d/2c} \text{Re}[E_z(z,t)] dt \\ &= \frac{1}{d} \int_{-d/2c}^{d/2c} \text{Re}[E_z(z)]_{beam} e^{j(\omega t + \phi)} dt \\ &= \frac{1}{d} \int_{-d/2}^{d/2} \text{Re}[E_z(z)] \{ \text{Cos}(\beta_z z + \phi) + j \text{Sin}(\beta_z z + \phi) \} dz \\ &\quad (\text{for synchronous beam } \omega t - \beta_z z = 0) \\ &= \frac{1}{d} \int_{-d/2}^{d/2} E_z(z) \text{Cos}(\beta_z z + \phi) dz \end{aligned} \quad (5-12)$$

Let us here normalize the field as

$$\int |E|^2 dV = 1 \rightarrow U = \frac{\mathcal{E}}{2} \quad (5-13)$$

And define the field integration along the beam axis, z, as

$$\begin{aligned} E_{acc} &= \frac{1}{d} \int_{-d/2}^{d/2} E(z) \text{Cos}(\omega t) dz \\ E_0 &= \frac{1}{d} \int_{-d/2}^{d/2} E(z) dz \end{aligned} \quad (5-15)$$

and the transit time factor as

$$T = E_{acc} / E_0 \quad (5-16)$$

then the impedance becomes

$$\frac{R}{Q} = \frac{1}{d} \frac{(E_{acc} d)^2}{2\omega U} = \frac{E_{acc}^2}{2\omega(U/d)} = \frac{2d Z_0}{2\omega/c} E_{acc}^2 \quad (5-17)$$

In the previous field expression of a pillbox mode,

$$\begin{aligned} \int |E|^2 dV &= A_{nl}^2 \\ A_{n0}^2 &= \pi d a^2 J_1^2(\rho_{0n}) \quad \text{for } l=0 \\ A_{nl}^2 &= \pi d a^2 J_1^2(\rho_{0n}) \frac{1}{2} \left\{ 1 + \left( \frac{l\pi a}{d \rho_{0n}} \right)^2 \right\} \quad \text{for } l \neq 0 \end{aligned} \quad (5-18)$$

Then to adjust the normalization to this section, we should express as

$$E_z(z) = \frac{1}{A_{nl}} \text{Cos}(m\theta) J_m(K_c r) \text{Cos}(\beta_z z) \quad (5-19)$$

For TM<sub>010</sub> mode,

$$E_{010,z}(z) = \frac{1}{A_{10}} J_0(r=0) = \frac{1}{A_{10}} \quad (5-20)$$

Finally we get

$$\begin{aligned} E_{acc} &= \frac{J_0(r=0)}{A_{10} d} \int_{-d/2}^{d/2} \text{Cos}\left(\frac{\omega}{c} z + \phi_s\right) dz = \frac{J_0}{A_{10} d} \frac{2c}{\omega} \text{Sin}\left(\frac{\omega d}{2c}\right) \text{Cos} \phi_s \\ T &= \frac{2c}{\omega d} \text{Sin}\left(\frac{\omega d}{2c}\right) \text{Cos} \phi_s \\ \frac{R}{Q} &= \frac{2d Z_0}{\omega/c} \left( \frac{2c J_0}{A_{10} d \omega} \right)^2 \text{Sin}^2\left(\frac{\omega d}{2c}\right) \text{Cos}^2 \phi_s \end{aligned} \quad (5-21)$$

This equations are used for estimating the accelerating mode in TM<sub>010</sub> mode. For TM<sub>0nl</sub> mode, the expressions are as follows.

$$\begin{aligned} E_{acc} &= \frac{J_0}{A_{nl} d} \int_{-d/2}^{d/2} \text{Cos}\left(\frac{\ell\pi}{d} z\right) \text{Cos}\left(\frac{\omega}{c} z + \phi_s\right) dz \\ &= \frac{J_0 \text{Cos} \phi_s}{A_{nl} d} \left[ \frac{\text{Sin}\left(\frac{\omega}{c} + \frac{\ell\pi}{d}\right) \frac{d}{2}}{\frac{\omega}{c} + \frac{\ell\pi}{d}} + \frac{\text{Sin}\left(\frac{\omega}{c} - \frac{\ell\pi}{d}\right) \frac{d}{2}}{\frac{\omega}{c} - \frac{\ell\pi}{d}} \right] \\ &= \frac{2\omega J_0 \text{Cos} \phi_s}{A_{nl} d c} \frac{1}{\left(\frac{\omega}{c}\right)^2 - \left(\frac{\ell\pi}{d}\right)^2} B_l \end{aligned} \quad (5-22)$$

where

$$\begin{aligned} \text{where } B_l &= \cos\left(\frac{\ell}{2}\pi\right)\sin\left(\frac{\omega d}{2c}\right) \text{ for } \ell = \text{even} \\ &= \sin\left(\frac{\ell}{2}\pi\right)\cos\left(\frac{\omega d}{2c}\right) \text{ for } \ell = \text{odd} \end{aligned} \tag{5-22'}$$

These are the very basic estimation used to estimate the realistic cavity based on the pillbox assumption.

## 6. Circuit modeling of a cavity

### 6.1 Cavity field to equivalent circuit

The representation of the cavity field with lumped electric resonant circuit parameters is made for the  $TM_{010}$  mode in a pillbox cavity as shown in Fig. 24 below.

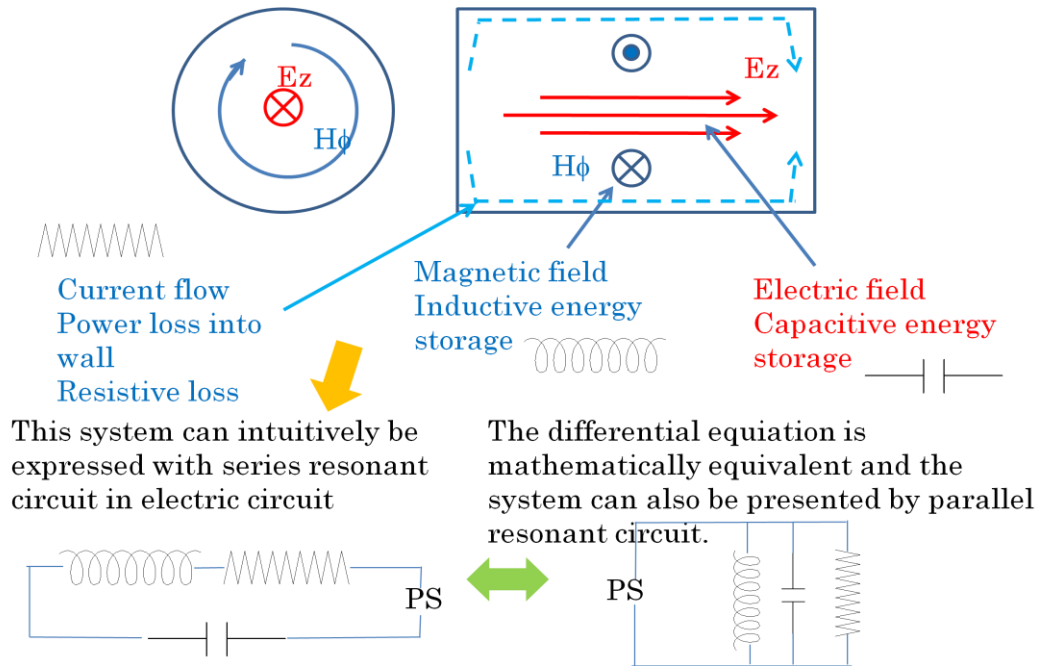


Fig. 24 Cavity field representation with lumped circuit elements.

By expressing the cavity with such a lumped electric resonant circuit, the whole RF system including the power generation and power transmission line can be represented by the similar circuit. Below shows the Figure taken from P. Wilson's lecture<sup>13</sup>.

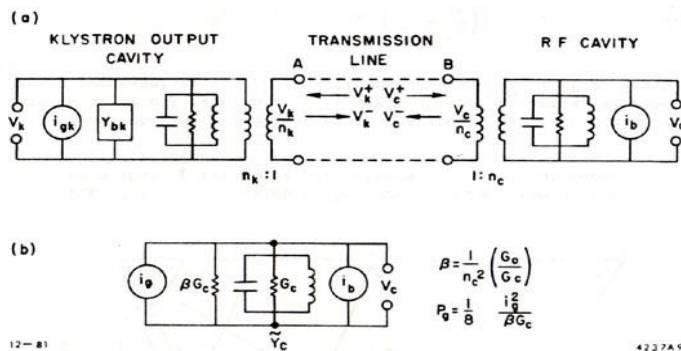
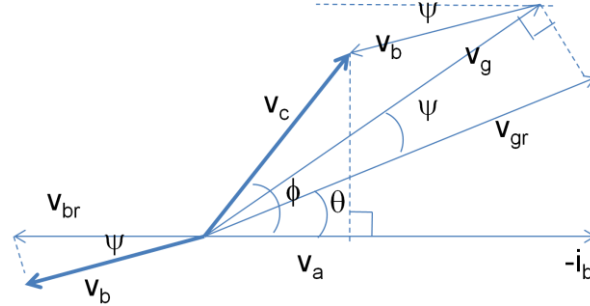


Fig. 3.9. (a) Equivalent circuit for a beam-loaded cavity coupled to a klystron; (b) simplified circuit assuming a matched RF source.

Fig. 25 RF system representation by lumped element.

## 6.2 Cavity response expression in the phaser diagram

The cavity system behaves as an electric resonant circuit and various characteristics are derived from circuit analysis. It is convenient to express the field in the cavity by phaser, as shown in Fig. 26. Here we extract the complex vector from actual field by dropping the  $\exp(j\omega t)$  term.



Phasor diagram

Fig. 26

The definition of phaser angle can be set with respect to the beam as

shown in the figure. Here the beam leaves the negative field  $V_{br}$  and this becomes the reference angle. If the cavity is excited by the generator voltage  $V_{gr}$ , the cavity excited field is rotated by an angle  $\psi$ , where the parameter is estimated as

$$\tan \psi = -2Q_L \delta \quad \text{where} \quad \delta = (\omega - \omega_0) / \omega_0 \quad (6-1)$$

This is called as the tuning angle. Even if the external RF source excites the cavity with some frequency off from the resonant one, the free oscillation in the cavity makes the rotation of the cavity excited field. It represents how much the frequency is off from resonant one with respect to the Q width of the cavity. The beam comes synchronously with RF so that the beam induced field also rotates by the same amount  $\psi$ . The actual cavity field  $V_c$  is formed as the superposition of the excited field and beam induced field as shown in Fig. 26.

## 6.3 Transient response

Let us consider the response of a cavity responding to the square pulse. From energy conservation,

$$E_{out} = E_e + \Gamma E_{in} \quad , \quad P_{in} = P_{out} + P_c + \frac{dU_c}{dt} \quad , \quad (6-2)$$

where  $E_{out}$ ,  $E_e$  and  $E_{in}$  are the outgoing wave from cavity, the emitted wave from cavity stored field and the reflected wave from the cavity responding to the incident of power incident to the cavity. The reflection coefficient is  $\Gamma$ . The power relation in the second equation states simply that the incident power into the cavity equals the sum of out-going power, cavity wall loss and the rate of increase of the cavity stored energy.

The reflection coefficient  $\Gamma$  is almost -1 and the coupling of the input circuit to the cavity is expressed as

$$\beta_c \equiv \frac{P_{out}}{P_c} \quad (6-3)$$

where it is the ratio of outgoing wave w.r.t. cavity wall loss. The typical cavity response time,  $t_c$ , is expressed as

$$t_c \equiv \frac{2Q_L}{\omega} = \frac{2Q_c}{(1 + \beta_c)\omega} \quad (6-4)$$

then the above energy / power equation becomes

$$t_c \frac{dE_e}{dt} + E_e = \frac{2\beta_c}{1 + \beta_c} E_{in} \quad (6-5)$$

Therefore, the emission from cavity stored field can be written as

$$E_e = \frac{2\beta_c}{1 + \beta_c} E_{in} (1 - e^{-t/t_c}) \quad (6-6)$$

The emitted field from cavity becomes

$$E_{out} = E_e - E_{in} = \frac{2\beta_c}{1 + \beta_c} E_{in} (1 - e^{-t/t_c}) - E_{in} \quad (6-7)$$

Therefore, the cavity stored field becomes

$$V(t) = (1 - e^{-t/t_c}) \sqrt{\left(\frac{R}{Q}\right) \omega t_c P_{in} \frac{2\beta_c}{1 + \beta_c}} \quad (6-8)$$

Various cases exist depending on the coupling of the input circuit to the cavity can be calculated by this equation. Some of the results are shown in Fig. 26.

When we take the beam loading into account, the power relation becomes

$$P_{in} = P_{out} + P_c + \frac{dU_c}{dt} + I_b V_a \quad (6-9)$$

If the beam injected to the cavity at a proper timing,

$$\frac{dU_c}{dt} + I_b V_a = 0 \quad (6-10)$$

can be satisfied so that the accelerating voltage does not change. If we modify the  $P_{in}$  in a proper manner, the injection timing and beam current can be set as we want. This is the beam loading compensation of the cavity field.

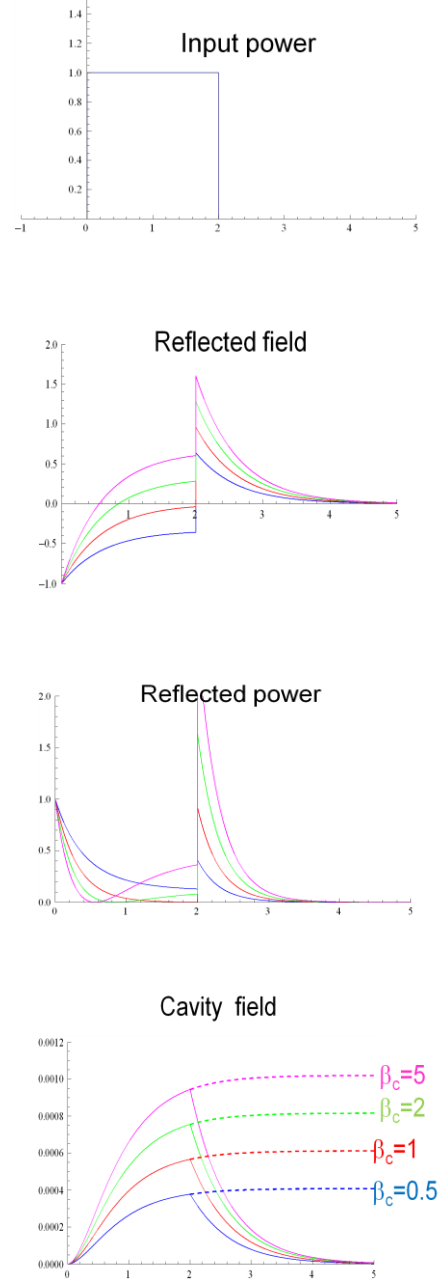


Fig. 26

## 7 Travelling wave linac

### 7.1 SW and TW

As seen in section 5.1 for pillbox mode expression, the electric field of a SW resonant mode is 90 degree different from the magnetic field. This behavior can be understood as shown in Fig. 27. The  $E_z$  and  $H_\phi$  are shown schematically in the figure and these two vectors are related by the Maxwell's equation shown in the figure. Time derivative gives 90 degrees difference. This means the electric field becomes maximum when magnetic field is zero and vice versa. The SW field is described as below.

$$SW: e^{j\omega t} \sin(kz), e^{j\omega t} \cos(kz) \quad (7-1)$$

On the other hand, the TW mode is expressed as

$$TW: e^{j(\omega t - kz)}, e^{j(\omega t + kz)} \quad (7-2)$$

and the fields are expressed as shown in the section 2.2. Here the electric field and magnetic field in a transverse direction is in phase. This is needed for non-zero poynting vector along the transmission line allowing the power flow.

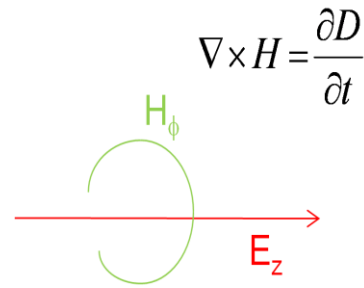


Fig. 27

Once we have the SW field and TW one expressed such as above, these are related with each other by a manipulation as below.

$$\begin{aligned} TW: e^{j(\omega t - kz)} \pm e^{j(\omega t + kz)} &\rightarrow SW: e^{j\omega t} \cos(kz) \text{ or } e^{j\omega t} \sin(kz) \\ SW: e^{j\omega t} [\cos(kz) \pm j \sin(kz)] &\rightarrow TW: e^{j(\omega t - kz)} \pm e^{j(\omega t + kz)} \end{aligned} \quad (7-3)$$

In Fig. 28 are shown two SW modes with  $2\pi/3$  phase advance per cell with shorted condition and open condition at the two ends, corresponding to Cos and Sin form. If we combine these two SW as described in the above equation, the TW mode can be obtained as shown in Fig. 29. In this figure, eight snap shots of the TW mode within an half RF cycle are shown.

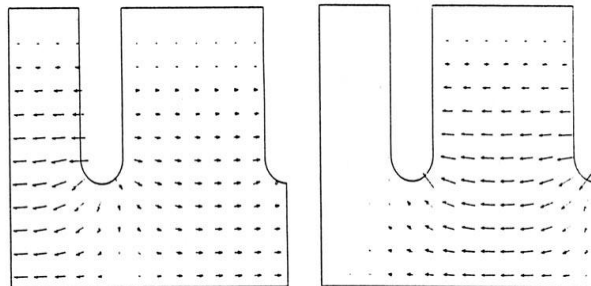


Fig. 28  $2\pi/3$  SW modes.



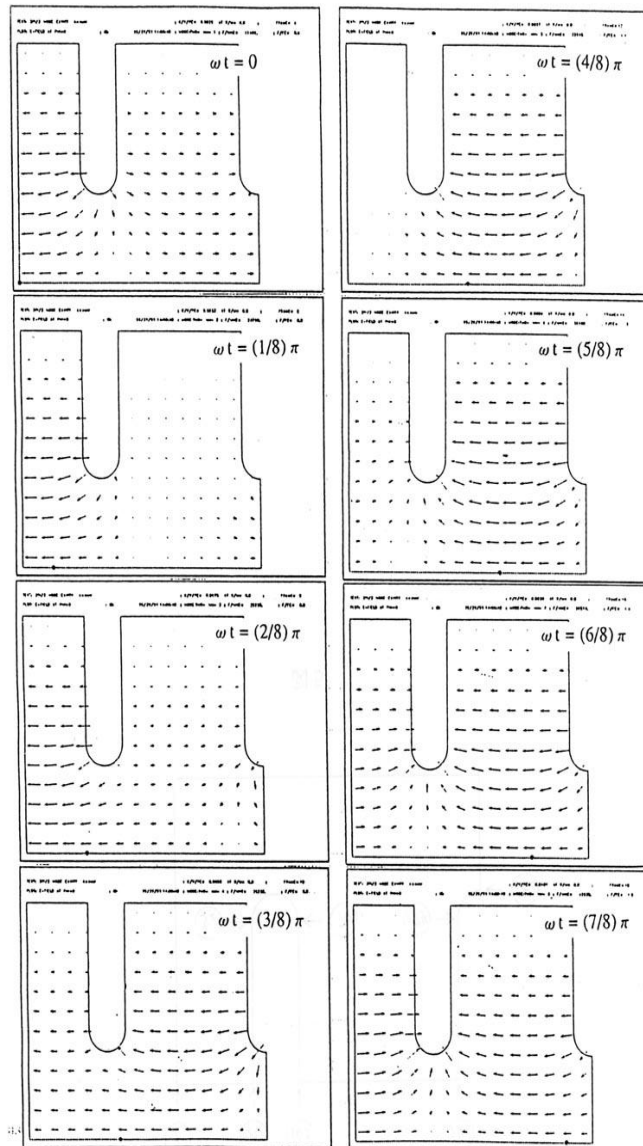


Fig. 29 TW 2p/3 mode: Snap shot at 8 time slot in half cycle.

It is to be noted that the shunt impedance of the TW mode is twice of SW mode, because the acceleration occurs with a space harmonic component synchronous to the beam, in the direction of beam travelling, but the stored energy for SW need the travelling wave in both directions.

The ILC adopted long pulse SW utilizing the low loss cavity but it is possible to adopt TW mode by circulating the exit wave back to the input port through an external circuit, though it may be difficult to realize it outside main cavity in a superconducting cavity system.

On the contrary, the NCC cavity usually adopts TW to make the structure length long and reduce the number of input circuits. In this case, the power left at the end of structure should be terminated

by the outside load. The situation is not good from power transfer efficiency point of view. On the other hand, if the accelerating gradient is set very high, breakdowns occur and this becomes one of the limiting parameters for the TW linac accelerator gradient. In reality, the energy deposited in a very small spot by arcing will be large for the TW case than SW case, because the incident power comes anyway near or to the breakdown cell in the TW structure. This may destroy the cavity inner surface through many breakdowns during a long-term operation. However, the usage of the TW is still attractive for reaching very high gradient and this is why the following sections of this lecture serve for it.

## 7.2 Acceleration in TW linac and related parameters

In the TW linac, the beam is accelerated by the interaction with the power flow along the beam axis. This power flow is attenuated as it propagates but this attenuation behavior is one of the key parameters to characterize the system as will be described from now.

There are two basic design categories, CZ, constant impedance design, and CG, constant gradient design. If we take some other cares than the acceleration such as the higher modes, there are lots of design cases in choosing the profile of the accelerating field along the structure. However, in most cases, the profile is similar to CG so that the analyses based on CZ and CG are the basic to understand the TW linac.

It is important to synchronize the RF propagation field to the beam. For this purpose, much cares are taken for tuning the structure. The input and output port, where the transformation of the propagating mode take place, is also a key element in design and making the structure. In this chapter, we review the relevant ideas and treatments of TW linacs in its regular section other than input/output region.

The travelling wave, a propagation of a microwave, is expressed as below in its longitudinal electric field component which acts as an acceleration / deceleration mechanism.

$$\begin{aligned}
 E_z(r, \theta, z, t) &= \sum_{n=-\infty}^{n=\infty} E_p(r, \theta, z) e^{j\omega t - \gamma z} \\
 &= \sum_{n=-\infty}^{n=\infty} E_n(r, \theta) e^{j(\omega t - \beta_n z)} e^{-\alpha z}
 \end{aligned} \tag{7-4}$$

where

$$\beta_n = \beta_0 + 2\pi n / d$$

$$E_n(r, \theta) = \frac{1}{d} \int_z^{z+d} E_d(r, \theta, z) e^{j(2\pi n/d)z}$$

Here the infinite number of space harmonics contribute to the formation of the travelling wave mode. Red dots in Fig. 8 is plotted such space harmonics. The contribution to the net acceleration for a long

distance is only from  $m=0$ , which is synchronous to the beam phase velocity. In a more practical way, it is expressed as

$$E_z(r, \theta, z, t) = \sum_{n=-\infty}^{n=\infty} a_n J_0(k_m r) e^{j(\omega t - \beta_n z)} \quad (7-5)$$

where  $\beta_n = \beta_0 + 2\pi n/d$  and  $k_m^2 = k^2 - \beta_n^2$

Many of the relevant parameters in TW linac can be understood by those of SW case described in chapter 3 with the corresponding relationship as shown below.

| SW                               | TW                             |
|----------------------------------|--------------------------------|
| Acceleration voltage in a cavity | Acceleration gradient          |
| Stored energy in a cavity        | Stored energy in a unit length |
| Power loss in a cavity           | Power loss in a unit length    |

In practice, three most important parameters are expressed as

$$r \equiv \frac{E_a^2}{|dP/dz|} \quad Q \equiv \frac{\omega u}{|dP/dz|} \quad r/Q \equiv \frac{E_a^2}{\omega u} \quad (7-6)$$

The power flow is equal to the energy density per unit volume times the group velocity, it is expressed as

$$P \equiv v_g \cdot u \quad \text{with} \quad v_g = d\omega/d\beta \quad (7-7)$$

and the attenuation characteristics are expressed as below.

$$\frac{dP}{dz} = -2\alpha P \quad \frac{dE_a}{dz} = -\alpha E_a \quad \alpha \equiv \frac{\omega}{2v_g Q} \quad (7-8)$$

Here  $\alpha$  is the attenuation parameter with unit of [1/m]. It is related to the group velocity and the Q value of the structure. Then, the field and power flow is attenuated as

$$E_a = E_0 e^{-\alpha z} \quad P_a = P_0 e^{-2\alpha z} \quad (7-9)$$

This is the very basic of the TW structure. If we calculate the field, power and total attenuation along a structure of the length  $L$ , we get

$$E_L = E_0 e^{-\alpha L} \quad P_L = P_0 e^{-2\alpha L} \quad \tau \equiv \alpha L = \frac{\omega L}{2v_g Q} \quad (7-10)$$

here we call  $\tau$  as the attenuation parameter of the structure.

From here we focus on DLS, disk loaded structure, which is most widely used for the high energy electron linac. Firstly the phase advance per cell characterizes the mode. The dispersion relation is as usual and shown in Fig. 30.

The choice of the mode is determined by the dispersion characteristics of the structure and the operation frequency. In Fig. 31 are shown some of the mode patterns. The fields shown in the figure are those of the SW mode, because the calculated field in SW can serve to calculate the basic parameters of the TW mode with some SW-TW relationship in mind and also the SW field can be expressed as real number and is easy to visualize. The field pattern can also be understood from the SW field pattern. These SW patterns appear in TW in each 90 degrees in RF cycle.

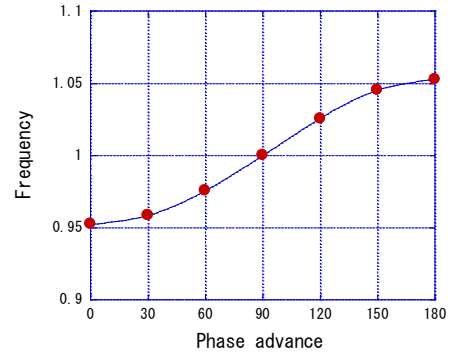


Fig. 30

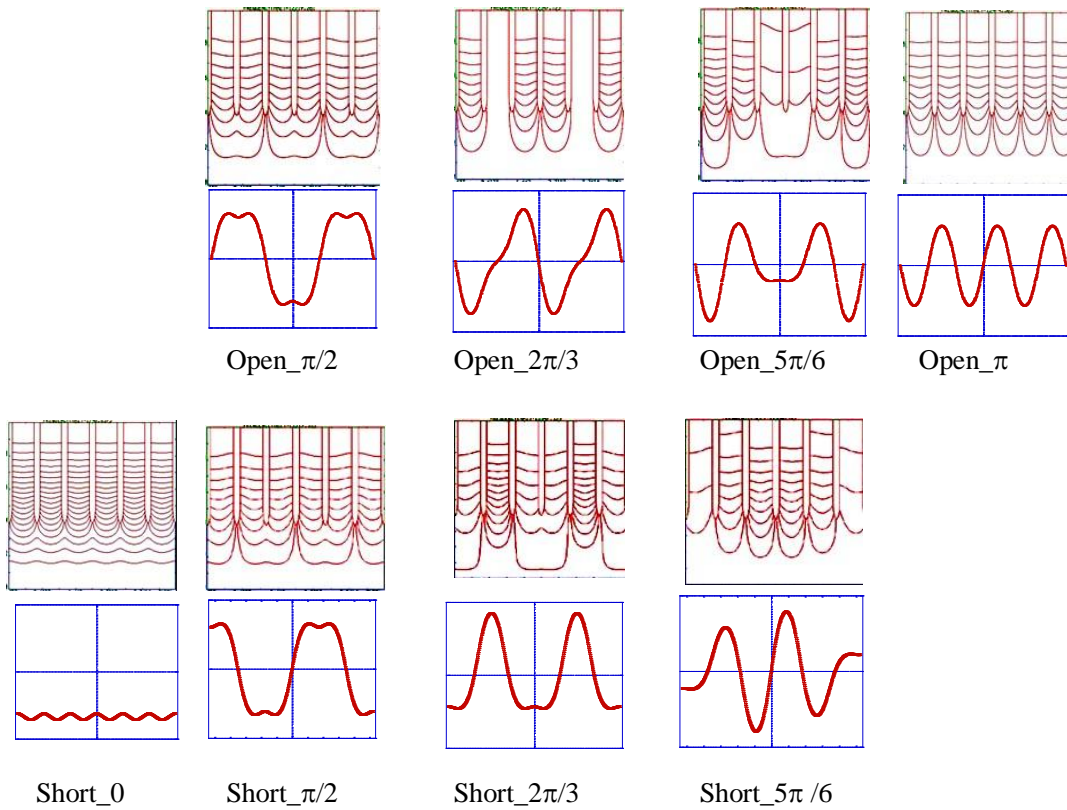


Fig. 31 SW mode pattern and on axial field on axis for DLS.

### 7.3 Modes in DLS, disk-loaded structure

For the actual design of DLS, the parameters (a,b,t) are the most basic parameters as shown in Fig. 32. The disk pitch,  $d$ , is determined from frequency  $F$  and mode  $\phi$  phase advance per cell,

$$d = \lambda \frac{\phi}{2\pi} \quad (7-11)$$

where  $\lambda$  is wave length in free space.

In Fig. 33(a), the on-axis  $E_z$  field of  $2\pi/3$  mode SW is plotted<sup>11</sup>. Also those plotted in the same figure are the space harmonics decomposed from this SW mode by Fourier transformation. The beam can get net energy only from the mode  $m=0$  with the coefficient  $a_0$  in the figure. The TW impedance is calculated essentially by deducing this term from the Fourier integral

$$\frac{1}{d} \int_0^d E_d(z) e^{j\beta_0 z} dz \quad (7-12)$$

The impedance this calculated for various phase advance per cell is plotted in Fig.33(b)<sup>11</sup>. Here the variable is the number of disks per free space wavelength. The broad maximum is identified which is equivalent to the  $2\pi/3$  phase advance per cell. Therefore, many of the TW accelerator with DLS take this mode for its acceleration mode.

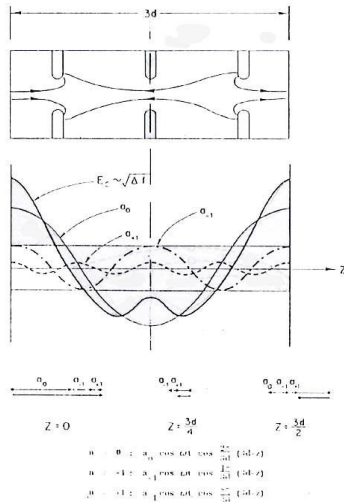


Fig. 26. Example of three cavity stack resonating in  $2\pi/3$  mode with illustration of how first three space harmonics add and subtract to give cavity field observed by beam measurement. The perturbation  $\delta f$  is proportional to  $E_z^2$ .

Fig. 33 (a)

Space harmonic component.

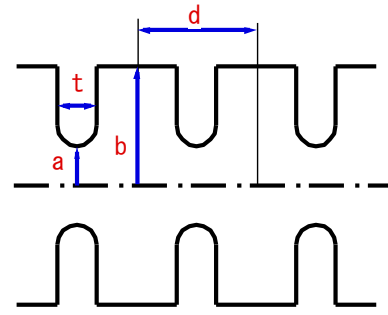


Fig. 32

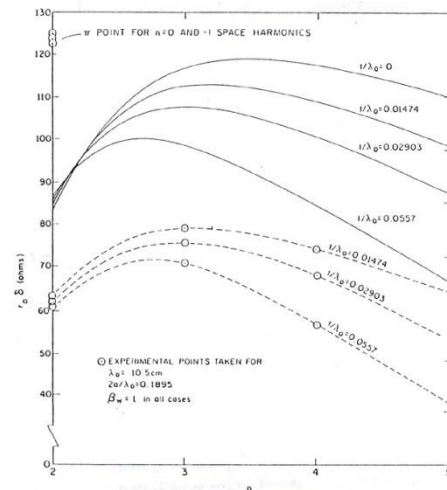


Fig. 27. Theoretical and experimental curves of normalized shunt impedance ( $r_0 \beta$ ) vs. number of disks per wavelength ( $n$ ) for various values of  $t/\lambda_0$  at  $\beta_w = 1$ .

Fig. 33(b)

Impedance versus disks / wavelength

### 7.4 DLS basic design variables

In the Fig. 34 are shown various parameters of the  $2\pi/3$  mode in DLS calculated by numerical simulation code, SUPERFISH.

The parameter ‘b’ is automatically determined from tuning of the frequency. The Q value increases as thickness decreases. The group velocity  $v_g$  increases as aperture increases or the thickness decreases and this behavior can intuitively understood because the group velocity is the ratio of propagation power to the stored energy, where the latter increases as reducing the power flow by reducing the leakage of power through the disk aperture. The shunt impedance, r and also  $r/Q$ , both increase as thinner disk thickness. However, the thin disk (smaller t) will make the  $E_s/E_{acc}$  larger because of the field concentration is towards the disk opening and the radius of the curvature is usually set to  $t/2$ , a half of the disk thickness. The  $E_s/E_{acc}$  increases also for larger ‘a’ because the field concentration toward beam axis is less for larger aperture. The actual DLS design should be done with these characteristics in mind.

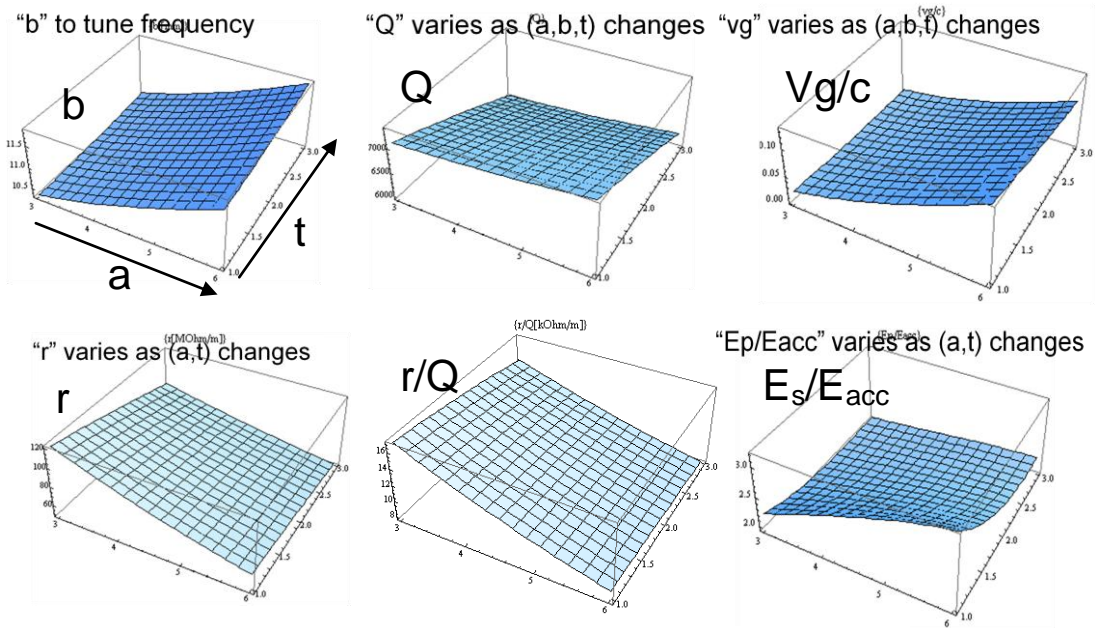


Fig. 34 Parameters of  $2\pi/3$  mode as function of (a,t).

### 7.5 Energy gain expression, especially CG case

In many of the DLS structures, the constant gradient (CG) structure type is usually taken. This is because the  $E_{acc}$  is kept constant as its name states and it is reasonable to take this design if we consider the arcing which is related to high  $E_s$  field along the structure, while the  $E_s$  is roughly speaking 2 times higher than  $E_{acc}$ . Since the  $E_{acc}$  is determined from  $dP/dz$ , the CG design is realized by

$$|dP/dz| = \text{const} \Rightarrow \frac{P(z)}{P_0} = 1 - (z/L)(1 - e^{-2\tau}) \quad (7-13)$$

in case of neglecting small variation of  $r$  along the structure. If we explicitly write the formula,

$$E_{acc} = \sqrt{\frac{\omega r}{v_g Q} P} \quad (7-14)$$

we now tell that  $v_g$  should be scaled as  $P$ , which is linearly decreasing function of  $z$ .

$$v_g(z) = \frac{\omega L}{Q} \frac{1 - (z/L)(1 - e^{-2\tau})}{1 - e^{-2\tau}} \quad (7-15)$$

In this design the filling time is calculated as

$$T_f = \int_0^L \frac{dz}{v_g(z)} = \tau \frac{2Q}{\omega} \quad (7-16)$$

and this becomes equivalent to that of the constant impedance (CZ) design. An example of the CG design is shown in Fig. 35. Here the red line shown the actual constant design structure calculated by numerical code, while those of dashed lines are for the CG design described in this section with the  $v_g$  in a linear function of  $z$ . These two show fairly good agreement, meaning that many basic characteristics of the actual CG structure can be estimated from the simple pseudo CG structure described here.

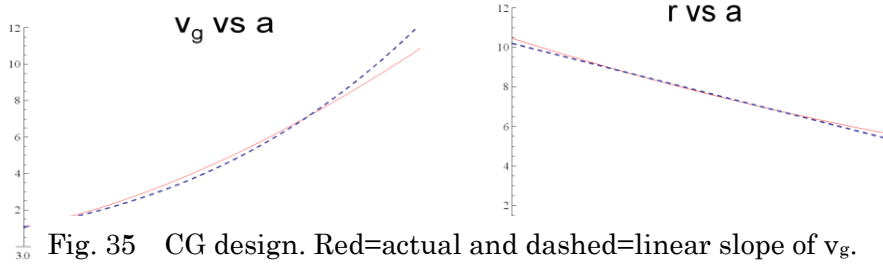


Fig. 35 CG design. Red=actual and dashed=linear slope of  $v_g$ .

Fig. 36 shows the actual design geometry along the DLS structure for GLC. The group velocity linearly changes from cell #10 to the last. In this area, the design is close to CG, while the initial part is intentionally modified from CG to reduce the electric field near input coupler region.

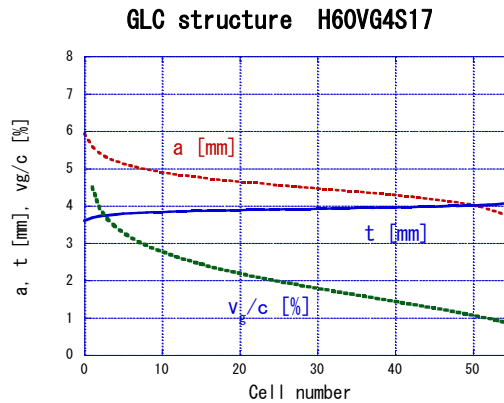


Fig. 36 Actual DLS design for GLC.

## 7.6 Beam loading

Let us calculate the energy gain of the TW structure. The actual field is the sum of the externally driven field and the beam loaded field. The former can easily be calculated as

$$\begin{aligned} CZ: V_0 &= (r L P_0)^{1/2} [(2/\tau)^{1/2} (1 - e^{-\tau})] \\ CG: V_0 &= (r L P_0)^{1/2} (1 - e^{-2\tau})^{1/2} \end{aligned} \quad (7-17)$$

Now consider the beam loaded field excited in an empty structure. The balance of the power flow along the structure and also the power left by the beam,

$$\frac{dP}{dz} = I_0 E_b - 2\alpha P \quad (7-18)$$

where the first term is the power from beam by deceleration field  $E_b$ , while the second term is related to the local power flow along the structure. Since

$$E_b^2 = 2\alpha r P \quad (7-19)$$

then

$$\frac{dE_b}{dz} = I_0 \alpha r - \alpha E_b + \frac{E_b}{2\alpha} \frac{d\alpha}{dz} \quad (7-20)$$

and this equation becomes simple when we assume CZ or CG structure type.

$$\begin{aligned} CZ \text{ case: } \frac{dE_b}{dz} &= I_0 \alpha r - \alpha E_b \\ CG \text{ case: } \frac{dE_b}{dz} &= I_0 \alpha r \end{aligned} \quad (7-21)$$

By integrating these, we get the beam induced field along the structure. These are plotted in Fig. 37.

$$\begin{aligned} CZ: E_b(z) &= I_0 r (1 - e^{-\alpha z}) \\ CG: E_b(z) &= -\frac{I_0 r}{2} \ln \left( 1 - \frac{1 - e^{-2\tau}}{L} z \right) \end{aligned} \quad (7-22)$$

Then we can integrate these to get the beam loaded voltage for the whole structure.

$$\begin{aligned} CZ: V_b &= I_0 r L \left[ 1 - \frac{(1 - e^{-\tau})}{\tau} \right] \\ CG: V_b &= I_0 r L \left[ \frac{1}{2} - \frac{\tau e^{-2\tau}}{1 - e^{-2\tau}} \right] \end{aligned} \quad (7-23)$$

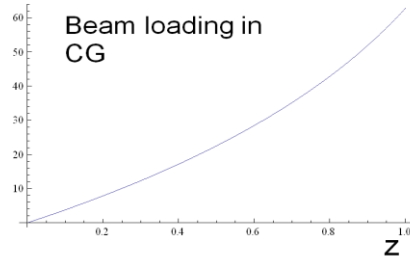
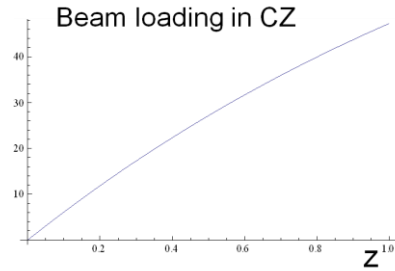


Fig. 37 Beam loaded field.

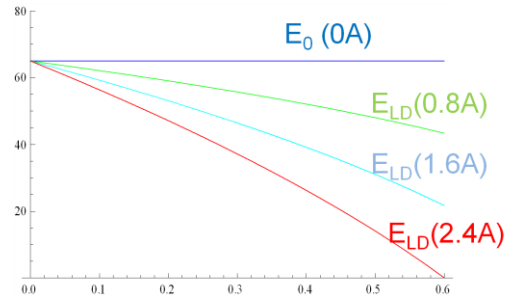


Fig. 38 Beam loaded field in CG.



The net total acceleration field becomes

$$CZ, CG: V_{LD} = V_0 \cos \theta - V_b \quad (7-24)$$

If the beam current increases, the loading increases linearly. The beam loaded gradient of various current are shown in Fig. 38 assuming CG with the shunt impedance of  $60\text{M}\Omega/\text{m}$ ,  $\tau=0.6$ ,  $E_{NL}=65\text{MV}/\text{m}$  and  $I_0 = 0, 0.8, 1.6$  and  $2.4\text{A}$ .

In Fig. 39 is shown the gradient without beam ( $E_{NL}$ ) and that with beam of  $0.9\text{A}$  ( $E_{LD}$ ) for the structure shown in Fig. 36. It is to be noted that the beam loaded gradient decreases toward the downstream of the structure. We may design the structure with the beam loaded gradient to be flat.

If the beam current increases,  $V_b$  increases linearly and it finally cancels the externally driven field completely. It happens in fully loaded operation such as shown in Fig. 38 with  $2.4\text{A}$  current. This kind of operation is needed for the system aiming at very efficient acceleration such as proposed for CLIC. An experimental proof<sup>14</sup> is shown in Fig. 40.

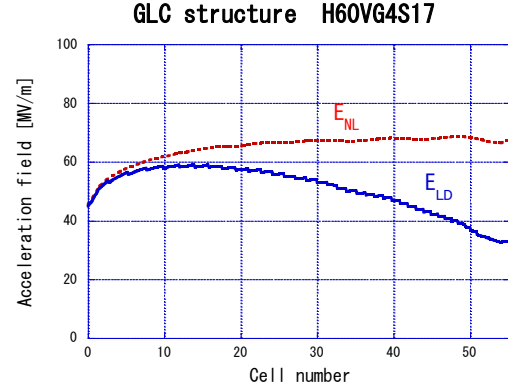


Fig. 39 Actual beam loaded field.

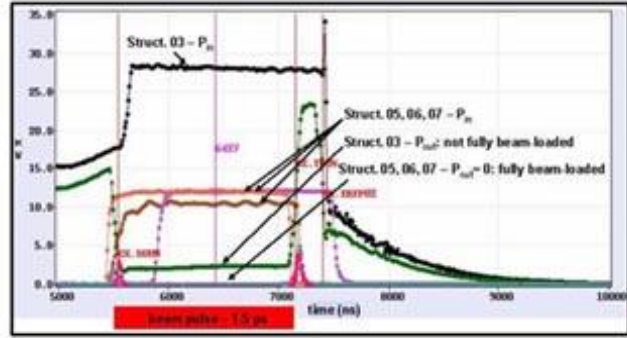


Figure 5: RF power levels at the structure input and output for always one accelerating structure per module as a function of time.

Fig. 40 CTF3 fully loaded operation.

### 7.7 Transient properties of microwave propagation

It is necessary to note that the TW linac fed with a fast rise pulse suffer from the dispersive effect when passing the structure.

$$\begin{aligned} E_0(t) &= \text{Re} \int_0^t e^{j\omega t} h(t) \\ E_q(t) &= \text{Re} \int_0^t e^{j\omega(t-\tau)} G_q(\tau) d\tau \\ &= Z_q(t) \text{Cos}(\omega t - \pi q - \varphi) \end{aligned} \quad (7-25)$$

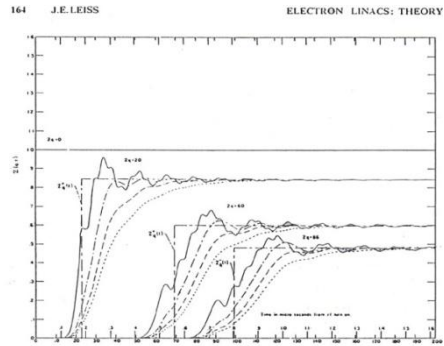


Fig. 5. Pulse transmission (Leiss *et al.* [1963]) in a specific  $2\pi/3$  mode S-band accelerator of 86 disks for different values of input risetime, plotted against time in units of  $\omega t$ . The amplitude  $Z_q(t)$  is shown for the signal at different points in the waveguide. The solid curve corresponds to the solutions found in eqs. (4.16) to (4.20).  $Z_q^*(t)$  is calculated using eq. (4.21). Dispersive calculations similar to these but for a constant gradient waveguide are given in Ilicin [1966].

Fig. 41 from Linear Accelerators.

where the incident wave  $E_0(t)$  is square pulse. The transfer function, green function,  $G_q(\tau)$  which is the field at  $z=q$  along the structure. The calculated result is shown in Fig. 41<sup>11</sup>. The same results are shown in an equivalent circuit analysis<sup>15</sup>.

### 7.8 Actual fabrication of TW structure and tuning

Here we briefly list up the process of making the TW linac structure. The structure is frequently formed as an assembly of disks sliced with planes perpendicular to the beam axis. An example is shown in Fig. 42.

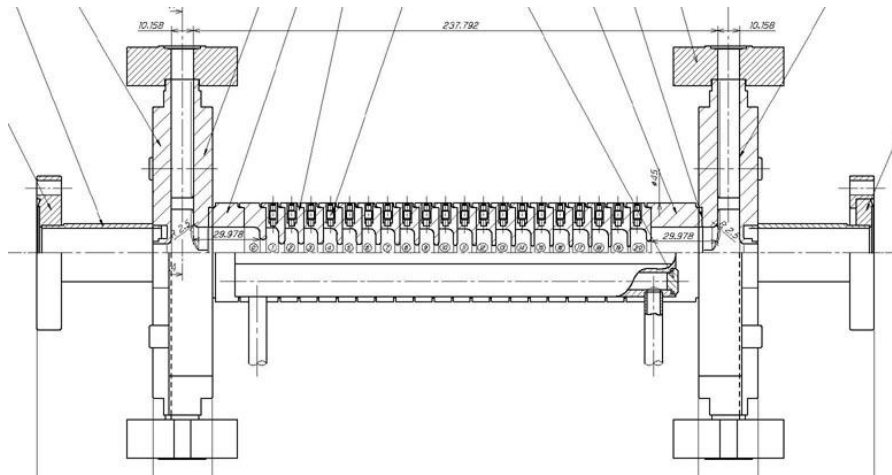


Fig. 42 TW structure based on stacking of sliced disks.

These disks are precisely machined and bonded. Then they are measured electrically and carefully tuned in frequency for the accelerating mode at least and sometimes also for higher modes.

Before closing the lecture, we show the calculation of the reflection due to the frequency error of cells for the accelerating mode. This is the basic idea how the frequency error changes the performance of the periodically loaded structure and makes it possible to get tolerances of the cells.

If there is a frequency error in cell  $m$  as shown in Fig. 43, a reflection occurs and it results in a transmission loss and phase error. This situation is formulated as the reflection coefficient  $R$  and the transmission coefficient  $T$  in the transmission line. Here the formula exists at the cell  $m$ .

$$T = 1 + R \quad (7-26)$$

The wave propagation along this transmission line is expressed as

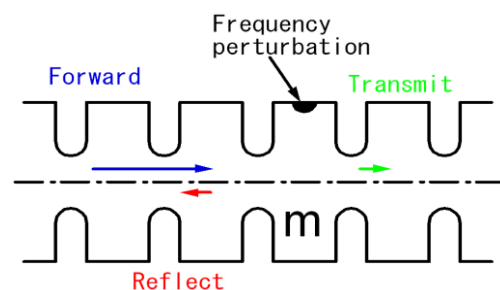


Fig. 43 from Linear Accelerators.

$$V_k = \begin{cases} 1e^{-k(j\theta+\Gamma)} + Re^{-2m(j\theta+\Gamma)} e^{k(j\theta+\Gamma)} & \text{for } k \leq m \\ Te^{-k(j\theta+\Gamma)} & \text{for } k > m \end{cases} \quad (7-27)$$

where  $V_k$  the field at cell  $k$ ,  $q$  is phase advance per cell and  $G$  transmission coefficient. From coupled resonator model treatment,

$$(\delta\omega_m^2 + \omega_m^2 - \omega^2 + j\frac{\omega\omega_m}{Q_m})V_m = \frac{1}{2}\omega_m^2(k_{m-1/2}V_{m-1} + k_{m+1/2}V_{m+1}) \quad (7-28)$$

and if we rewrite this using  $R$  and  $T$ , this becomes

$$\begin{aligned} (\delta\omega_m^2 + \omega_m^2 - \omega^2 + j\frac{\omega\omega_m}{Q_m})(Te^{-m(j\theta+\Gamma)}) &= \frac{1}{2}\omega_m^2 k_{m-1/2} (e^{-(m-1)(j\theta+\Gamma)} + e^{-2m(j\theta+\Gamma)} R e^{(m-1)(j\theta+\Gamma)}) \\ &+ \frac{1}{2}\omega_m^2 k_{m+1/2} T e^{-(m+1)(j\theta+\Gamma)} \end{aligned} \quad (7-29)$$

with proper cell frequency as

$$\delta\omega_m^2 + \omega_m^2 - \omega^2 + j\frac{\omega\omega_m}{Q_m} = \frac{1}{2}\omega_m^2 (k_{m-1/2} e^{-(m-1)(j\theta+\Gamma)} + k_{m+1/2} e^{-(m+1)(j\theta+\Gamma)}) \quad (7-30)$$

Therefore, the reflection coefficient  $R$  can be expressed as

$$R = \frac{\delta\omega_m^2 / \omega_m^2}{\delta\omega_m^2 / \omega_m^2 + k_{m-1/2}(\Gamma \text{Cos}\theta + j \text{Sin}\theta)} \quad (7-31)$$

Let us assume loss-less TW with  $2\pi/3$  mode propagation. If  $k \sim 0.02$  and  $\delta\omega^2/\omega^2 \sim 10^{-4}$ , then

$$R \approx \frac{\delta\omega_m^2 / \omega_m^2}{k_{m-1/2} \text{Sin}\theta} \approx \frac{10^{-4}}{0.02(\sqrt{3}/2)} \approx 10^{-2} \quad (7-32)$$

If this error is coherent over 10 cells, those cohere so that  $R$  becomes as much as 0.1. This amount of the systematic error,  $\delta\omega/\omega \sim 10^{-4}$  is not allowed. In contrast, random error makes square root nature in total and much smaller in total so that such amount of error is allowed. The above error in 12GHz is equivalent to  $1\mu\text{m}$  error in dimensions.

The frequency error results also in the associated the phase advance error due to the dispersive nature. In a singly coupled resonator chain model,

$$\omega = \frac{\omega_0}{\sqrt{1 + \kappa \text{Cos}(\phi)}} \quad (7-33)$$

So that

$$\frac{\partial\omega}{\partial\phi} = v_g = -\frac{1}{2}\omega_0 \kappa \text{Sin}(\phi) \quad (7-34)$$

Then the error in phase advance per cell  $\delta\Phi$  becomes

$$\delta\Phi = \delta\phi d = \frac{\delta\omega}{v_g} d = \frac{d/c}{v_g/c} \delta\omega = \frac{\lambda (\Phi/2\pi)/c}{v_g/c} \delta\omega = \frac{\Phi}{v_g/c} \frac{\delta\omega}{\omega} \quad (7-35)$$

The phase error is inversely proportional to  $v_g$ . If the phase advance per cell is 120 degree / cell, the 1MHz error gives 0.6 degree/cell. If this is systematic, it gives more than 10 degrees in total if 20cell structure such as in CLIC and better to be tuned out.

## References

- <sup>1</sup> M. Sands "Physics of Electron Storage Rings", Academic Press, 1971.
- <sup>2</sup> Y. Yamazaki and T. Kageyama, Part. Accel. 44 107 (1994).
- <sup>3</sup> I. Wilson and H. Henke, "The LEP main ring accelerator structure", CERN 89-09.
- <sup>4</sup> W. K. H. Panofsky and M. Phillips, "Classical Electricity and Magnetism", Addison-Wesley Publishing Company.
- <sup>5</sup> R. E. Collin, "Foundations for Microwave Engineering," McGraw-Hill, Kogakusha, Ltd.
- <sup>6</sup> E. Marcuvitz ed., "Microwave Handbook", p71, McGRAW-HILL BOOK Company, Inc., 1951.
- <sup>7</sup> J. C. Slater, "Microwave Electronics", D. van Nostrand co. Inc., 1950.
- <sup>8</sup> H. Padamsee, "Results on 9-cell ILC and 9-cell Re-entrant Cavities," PAC07, WEPMS-009, 1997.
- <sup>9</sup> H. Padamsee, J. Knobloch and T. Hays, "Superconductivity for Accelerators," John Wiley & Sons, Inc., 1998, ISBN 0-471-15432-6.
- <sup>10</sup> D. E. Nagle, E. A. Knapp and B. C. Knapp, "Coupled Resonator Model for Standing Wave Accelerator Tanks," Rev. Sci. Instr. 38, p1583, 1967, and E. A. Knapp, B. C. Knapp and J. M. Potter, "Standing Wave High Energy Linear Accelerator Structures," Rev. Sci. Instr. 39, p979, 1968.
- <sup>11</sup> P. M. Lapostolle and A. L. Septier ed., "Linear Accelerators," North-Holland Publishing Co., 1970.
- <sup>12</sup> J. Sekutowicz et al., "Superconducting Superstructure for TESLA Collider," EPAC98, p1876, 1998.
- <sup>13</sup> P. B. Wilson, "High Energy Electron Linacs: Application to Storage Ring RF System and Linear Colliders," SLAC-PUB-2884, 1982, Lecture given in 1981 Summer School, FNAL, 1981.
- <sup>14</sup> P. Urschütz et al., "Efficient Long-Pulse Fully Loaded CTF3 Linac Operation," LINAC06, Knoxville, ,
- <sup>15</sup> T. Shintake, p435, Joint US-Japan International School on Frontiers of Accelerator Technology, 1996, printed by World Scintific, 1996, ISBN 981-02-3838-X.